SANDIA REPORT

SAND2004-0939
Unlimited Release
Printed March 2004

Global Positioning System Pseudolite-Based Relative Navigation

Eric Monda

Prepared by
Sandia National Laboratories
Albuquerque, New Mexico 87185 and Livermore, California 94550

Sandia is a multiprogram laboratory operated by Sandia Corporation,
a Lockheed Martin Company, for the United States Department of Energy's
National Nuclear Security Administration under Contract DE-AC04-94AL85000.

Approved for public release; further dissemination unlimited.

Issued by Sandia National Laboratories, operated for the United States Department of Energy by Sandia Corporation.

NOTICE: This report was prepared as an account of work sponsored by an agency of the United States Government. Neither the United States Government, nor any agency thereof, nor any of their employees, nor any of their contractors, subcontractors, or their employees, make any warranty, express or implied, or assume any legal liability or responsibility for the accuracy, completeness, or usefulness of any information, apparatus, product, or process disclosed, or represent that its use would not infringe privately owned rights. Reference herein to any specific commercial product, process, or service by trade name, trademark, manufacturer, or otherwise, does not necessarily constitute or imply its endorsement, recommendation, or favoring by the United States Government, any agency thereof, or any of their contractors or subcontractors. The views and opinions expressed herein do not necessarily state or reflect those of the United States Government, any agency thereof, or any of their contractors.

Printed in the United States of America. This report has been reproduced directly from the best available copy.

Available to DOE and DOE contractors from
U.S. Department of Energy
Office of Scientific and Technical Information
P.O. Box 62
Oak Ridge, TN 37831

Telephone: (865)576-8401
Facsimile: (865)576-5728
E-Mail: reports@adonis.osti.gov
Online ordering: http://www.doe.gov/bridge

Available to the public from
U.S. Department of Commerce
National Technical Information Service
5285 Port Royal Rd
Springfield, VA 22161

Telephone: (800)553-6847
Facsimile: (703)605-6900
E-Mail: orders@ntis.fedworld.gov
Online order: http://www.ntis.gov/help/ordermethods.asp?loc=7-4-0#online

SAND2004-0939
Unlimited Release
Printed March 2004

Global Positioning System Pseudolite-Based Relative Navigation

Eric Monda
Graduate Student
Department of Aerospace Engineering
and Engineering Mechanics
The University of Texas
Austin, TX 78712-1085

Sandia Contract 03-1164

Abstract

Though the Global Positioning System has revolutionized navigation in the modern age, it is limited in its capability for some applications because an unobstructed line of sight to a minimum of four satellites is required. One way of augmenting the system in small areas is by employing pseudolites to broadcast additional signals that can be used to improve the user's position solution. At the Navigation Systems Testing Laboratory (NSTL) at NASA's Johnson Space Center in Houston, TX, research has been underway on the use of pseudolites to perform precision relative navigation. Based on the findings of previous research done at the NSTL, the method used to process the pseudolite measurements is an extended Kalman filter of the double differenced carrier phase measurements. By employing simulations of the system, as well as processing previously collected data in a real time manner, sub-meter tracking of a moving receiver with carrier phase measurements in the extended Kalman filter appears to be possible.

Acknowledgement

This research was funded by Sandia National Laboratories through a graduate research fellowship at the University of Texas at Austin, administrated by Sandia's Laboratory Directed Research and Development office.

TABLE OF CONTENTS

LIST OF FIGURES

CHAPTER 1
INTRODUCTION

1.1 THE HISTORY OF GPS

NAVSTAR, the Global Positioning System (GPS), draws its roots from the very earliest endeavors of mankind into space. In 1958, the same year that the United States launched its first satellite into Earth orbit, plans were being developed for the Transit satellite system. Transit would be used by the United States military, most significantly the U.S. Navy, to provide navigation services to ships and the submarines carrying the SLBM Polaris missiles that acted as a deterrent to massive nuclear strike on the American homeland.

While Transit performed its designed role for over 30 years from 1964 to 1996, it had scarcely been in service for 5 years before the Navy wanted to upgrade the system and the Air Force wanted to design their own. The existing Transit system had several shortcomings that the branches of the military wanted to correct in the improved version.[6] Its biggest shortcoming was that the user could be without any navigation information at all for up to 100 minutes, since only a small number of satellites in low orbits were in the constellation. Further, it required continuous tracking of the signal for the entire 10-20 minute pass and only after that time could a position be computed.[12] Further still, the system only worked well for slow moving objects, and the position fix was limited to two dimensions.

As Congress would not appropriate the funds required for development of different navigation systems for each branch of the military, the armed forces came together and decided upon a single system for all of them to use. In 1973, the general plan for the design of the GPS system was approved by the Department of Defense, and within 5 years the first satellite in the GPS constellation was launched. Tests were conducted of the system until 1995 when fully operational status was declared. Since that time, continued improvements and replacements to the GPS constellation have taken place.

1.2 GPS SYSTEM STRUCTURE

"GPS is a passive, time-of-travel-trilateration, navigation system." [9] This means that the user is able to compute their position without having to transmit, and does so by measuring the distance, either in meters or seconds, between themselves and a minimum of 4 other reference locations that have a position and transmission time that is known to that user. This brief sentence explains very simply, everything that makes the GPS system as valuable as it is today. A user with an inexpensive handheld receiver can, within a matter of seconds, find their position in three dimensions on the Earth to within about 10 meters and

know the current time to within tens of nanoseconds. Additional information such as the user's instantaneous velocity can be found from GPS measurements as well.

These reference stations with known positions and time are a constellation of between 24 and 30 satellites, (29 at the time of publication) that each orbit the Earth about 20,000 km from the surface. Each satellite is in an orbit that is inclined to the equator at an angle of 55 degrees and has an orbital period corresponding to one half of a sidereal day, 11 hours and 58 minutes. There are six orbital planes that one of these GPS satellites can reside in, and there are five slots within each plane for a satellite. Each satellite broadcasts its time and position by overlaying that information onto a specially coded pseudo-random noise (PRN) sequence such that all satellites can broadcast on the same frequency, and yet the messages from multiple satellites will not interfere with one another. An excellent and thorough description of the components and structure of the GPS system is provided by any number of sources.[1, 6, 12]

Yet, for all of its capabilities, the GPS system still has its weaknesses. Greatest among these is the fact that GPS signals are very weak, and therefore many objects including trees, buildings, terrain, and other metallic bodies in the direct path from the satellite to the receiving antenna can prevent the signal from getting through. As a result, there are applications where GPS does not work well.

1.3 PSEUDOLITES: THE NEED

There are a variety of terrestrial applications where GPS service is not available or is not as accurate as is required for the particular application. For example, a vehicle navigating between tall buildings in an urban environment may not be able to receive signals from a sufficient number of satellites. An aircraft doing an autonomous GPS landing would greatly benefit from having an additional signal just beneath it to greatly reduce the position solution error. A host of indoor applications in a warehouse, for example, could benefit from GPS, but the signals would not be received through the buildings walls. All of these applications would be facilitated with a capability to augment GPS coverage by placing another GPS signal transmitter at a location or locations on the Earth.

GPS augmentation is also desired in a variety of space-borne applications where it has been used more frequently in recent years.[10, 16, 19] Since GPS can provide instantaneous position and velocity solutions on-board a spacecraft, it is a far more efficient system to use than the previously method of tracking the satellite from the earth at numerous receiving stations and combining those measurements at another location to compute a solution that can be broadcast to the spacecraft. Naturally then, there are benefits of using GPS aboard the largest and most prominent manned space structure, the International Space Station (ISS).

Ideally, GPS could be used to control the rendezvous and docking of a spacecraft to the ISS. However, the size and structure of the ISS, as well as the maneuvers that are required for a spacecraft to dock with it, make it nearly impossible to use GPS alone to control the procedure. The ISS is comprised of many metal surfaces that are highly reflective to radio waves. Additionally, it is nearly 100 meters in length at this time, so a large volume

is created beneath the station where GPS signals may be blocked or degraded in quality. If a docking spacecraft approaches the ISS from below, this could mean a degradation of GPS service performance during the most critical phase of the docking as the GPS satellites reside far above the ISS and Space Shuttle. If GPS is to be used to control docking at the ISS, there must be some method of providing navigation services to spacecraft while they are close to and beneath the ISS.

1.4 PSEUDOLITES: WHAT ARE THEY?

Pseudolites transmit a signal that is similar to a GPS signal, but can be placed in a location to augment coverage to an area where the direct GPS service is not available. In the early days of GPS testing, before a full constellation was available, pseudolites were frequently used to help create a position fix. More recently, work with pseudolites has been performed extensively at Stanford University for a variety of applications. One example that has previously been implemented is a deep mining pit where vehicles at the bottom cannot see a sufficient arc of the sky to have continuous coverage, but can clearly receive signals from the inside walls of the pit.[17] In another application, pseudolites were used to improve the GPS position solution for landing aircraft autonomously.[3] Corrazini and How successfully navigated GPS pseudolites using carrier phase differential GPS when the integer ambiguity values were initialized and cycle slips were detected by an optical system.[5]

In addition to helping provide a receiver's absolute position, the pseudolite signal can be used to solve for a position relative to that transmitter, which is precisely what a docking spacecraft needs. One potential solution to the problem of GPS signal blockage during spacecraft rendezvous would be to attach several pseudolites to the underside of the ISS and allow a docking craft to use those signals to perform navigation relative to the station.

1.5 PREVIOUS WORK AT NSTL

The feasibility of this approach is currently being tested at the Navigation Systems & Technology Laboratory (NSTL) at the Johnson Space Center (JSC) in Houston, Texas. Two projects involving pseudolites that were previously examined in the NSTL are the AERCam, and the Ship Channel Receiver. The AERCam is a free flying robotic spacecraft that would navigate by differential GPS and perform inspection type tasks about the main spacecraft from which it was released.[21] The Ship Channel Receiver used pseudolite augmented GPS to find position and heading information for large ships in the Houston Ship Channel.[4] More information about the pseudolites used in this study is available in literature available from their manufacturer, IntegriNautics.[7, 8]

Over the past two years, Wawrzyniak and Smart, both at the University of Texas at Austin, have completed valuable research in May of 2001, and 2002, respectively, at the NSTL.[14, 20] Wawrzyniak examined a variety of navigation algorithms and found that the extended Kalman filter of double differenced carrier phase measurements processing method was the most robust of the algorithms examined, so long as motion exists to create observability of the system. Based on his findings, that algorithm is employed in this work.

Smart found that if dynamic selection of the reference pseudolite was employed, it may be possible to obtain results better than 1 meter in accuracy in real-time relative positioning. Creating that capability was the goal of this research. Both of their documents provide substantial background information about the NSTL lab and the pseudolite hardware that is employed in this study.

1.6 RESEARCH GOALS

Three specific contributions were completed in this research. The first was a modification of existing algorithms used by Wawrzyniak and Smart. These modified algorithms allow for dynamic selection of the reference pseudolite based on the signal to noise ratio (SNR) from each transmitting pseudolite and maintain integer ambiguity resolution and covariance values through switching of reference pseudolites. This switching of the reference pseudolite could be mandated by a change in the SNR values or a data dropout from the reference pseudolite. Previously, it had been observed that the reference pseudolite needed to be reassigned due to changes in signal strength. This phase would be concluded by testing and validating the new code with simulated data.

The second contribution involved testing the new code with data collected in the anechoic chamber near the NSTL last year by Smart. Though this data would be processed in a real-time manner, which is to say only information that was available in real-time was used to compute a solution, no truth trajectory was recorded in that data collection. As such, the computed solution cannot be compared to the truth to obtain a measure of the accuracy, but the general structure of the solution can be compared with knowledge of how the motion was generated.

The final achievement was to collect and process experimental data from the NSTL under a variety of receiver trajectories and signal tracking loops in the receiver software. By collecting a new set of data with trajectories generated and recorded by computers and a robot arm, a truth trajectory was maintained with which the computed motion could be compared and a measure of solution accuracy obtained. This would permit a metric of the system in the form of the accuracy of the system's position solution performance. The variety of trajectories and software tracking loops would illustrate system performance under different conditions.

1.7 REPORT OUTLINE

Based on the three phases of the research previously described, the report is split along very natural boundaries of the work. The first chapter provides the necessary background and history to lead into the current research. Chapter 2 examines the work done with the modified code on simulated data. Similarly, Chapter 3 explores the results from processing real data with that code. In Chapter 4, the results and difficulties of attempting to run the code in real-time at the NSTL are explored. Finally, this report concludes with a summary of the work and results, as well as recommendations to achieve the desired real-time capability.

CHAPTER 2
SIMULATION OF REAL-TIME CAPABILITY

2.1 CARRIER PHASE MEASUREMENTS AND DOUBLE DIFFERENCING

The carrier phase of the GPS signal provides a highly accurate measurement to be taken of the distance between a transmitter and receiver, but the measurement is made in terms of fractions of a single wavelength. Therefore, when using carrier phase measurements, no information is available regarding the integer number of wavelengths between the transmitter and receiver, but the fraction of a wavelength between is very well known. This is known as the integer ambiguity, and must additionally be resolved to compute a position solution of the receiver.

A model for the carrier phase measurement is presented in (1):

$$\Phi_A^j = \rho_A^j + c(\delta T^j - \delta t_A) + \lambda N_A^j + \varepsilon_A^j \tag{1}$$

where Φ_A^j is the distance between pseudolite j and receiver A, ρ_A^j is the carrier phase measurement between the two, c is the constant speed of light, δT^j is the clock offset of the pseudolite j, δt_A is the clock offset of receiver A, λ is the wavelength of the carrier phase (19.029 cm), N_A^j is the integer ambiguity across the same transmitter-receiver pair, and finally ε_A^j is the error on this measurement.

Clock offsets of both the receiver and transmitters can be eliminated by a technique of double differencing. A reference pseudolite must be selected and is normally chosen as the pseudolite providing the strongest signal since errors in that measurement would affect all others. The double difference measurement is made by subtracting single difference measurements made across the 2 receivers. The single differences are formed for each receiver by subtracting the measurement from the reference pseudolite, j, from the other receivers, k. The single difference then takes this form once the common receiver clock offset has been cancelled and omitted.

$$\Phi_A^k - \Phi_A^j = \rho_A^k - \rho_A^j + c(\delta T^k - \delta T^j) + \lambda(N_A^k - N_A^j) + \varepsilon_A^k - \varepsilon_A^j \tag{2}$$

which is simplified by introducing a differenced notation to (3):

$$\Phi_A^{jk} = \rho_A^{jk} + c\,\delta T^{jk} + \lambda N_A^{jk} + \varepsilon_A^{jk} \tag{3}$$

Forming the double difference by subtracting the single differenced measurements from a selected reference receiver, A, from the other receiver's measurements, B, removes the transmitter clock offsets and is simplified to (4):

$$\Phi_{AB}^{jk} = \rho_{AB}^{jk} + \lambda N_{AB}^{jk} + \varepsilon_{AB}^{jk} \tag{4}$$

These are the double differenced measurements which are processed by the extended Kalman filter. At each epoch where a signal is received from n pseudolites, n-1 measurements are available for processing as the measurement from the reference pseudolite is used to obtain the double differences and cannot be processed itself. The extended Kalman filter is a standard one incorporating process noise. For more information regarding Kalman filtering methods, the reader is referred to Poole and Tapley or numerous other texts on filtering methods. [13, 18]

2.2 LEGACY METHODS AND CODE

Through the cumulative work of Wawrzyniak, Smart, and others, a code was developed in both Matlab and C languages that can process the carrier phase measurements obtained by two receivers. With those raw measurements and knowledge of the location of a reference receiver, an accurate position solution of the second receiver's location relative to the reference receiver can be computed. The processing method for accomplishing this is an extended Kalman filter. The filter computes a state vector that includes elements representing the positions and velocities of the roving receiver in each of 3 dimensions, as well as the values for the double differenced integer ambiguity between the reference pseudolite and the other available pseudolites.

The previously employed code had several limitations that prevented it from being used in a real-time fashion. One major limitation of the existing code was an inability to perform dynamic selection of the reference pseudolite. As a result, previous data processing had required the user to examine the input data file and choose which pseudolite would be the reference for the entire run or command the reference pseudolite to change at a given epoch. This decision was based largely on consistent availability throughout the duration of data collection. Additional real-time shortcomings in the code were largely the result of this planned reliance on researchers to select the reference pseudolite *a priori*.

2.3 CODE MODIFICATIONS AND IMPROVEMENTS

Dynamic selection of the reference pseudolite was accomplished by means of the signal to noise ratio (SNR) data included with the incoming data stream. It is important that the most accurate available measurement is used to create the double differences since the data from that reference measurement will affect every double differenced measurement. As such, the strongest available signal, as measured by the highest SNR, is selected to be the reference pseudolite at the first epoch. After the first epoch, a Schmitt trigger, set to a value chosen by the user to create the level of reference pseudolite switching desired, is utilized to prevent excessive switching of the reference pseudolite when only small differences in the

relative SNR values between pseudolites exist. A block diagram of this algorithm is presented in Figure 1.

With the code modified to autonomously detect and change reference pseudolites, other changes needed to be made to the code as well. Under the previous structure, a change in the reference pseudolite reset the integer ambiguity to values based on the distance between the pseudolite and last computed position of the receiver. The previously solved integers are now used to compute the new values based on a different reference pseudolite. An example of this method is demonstrated:

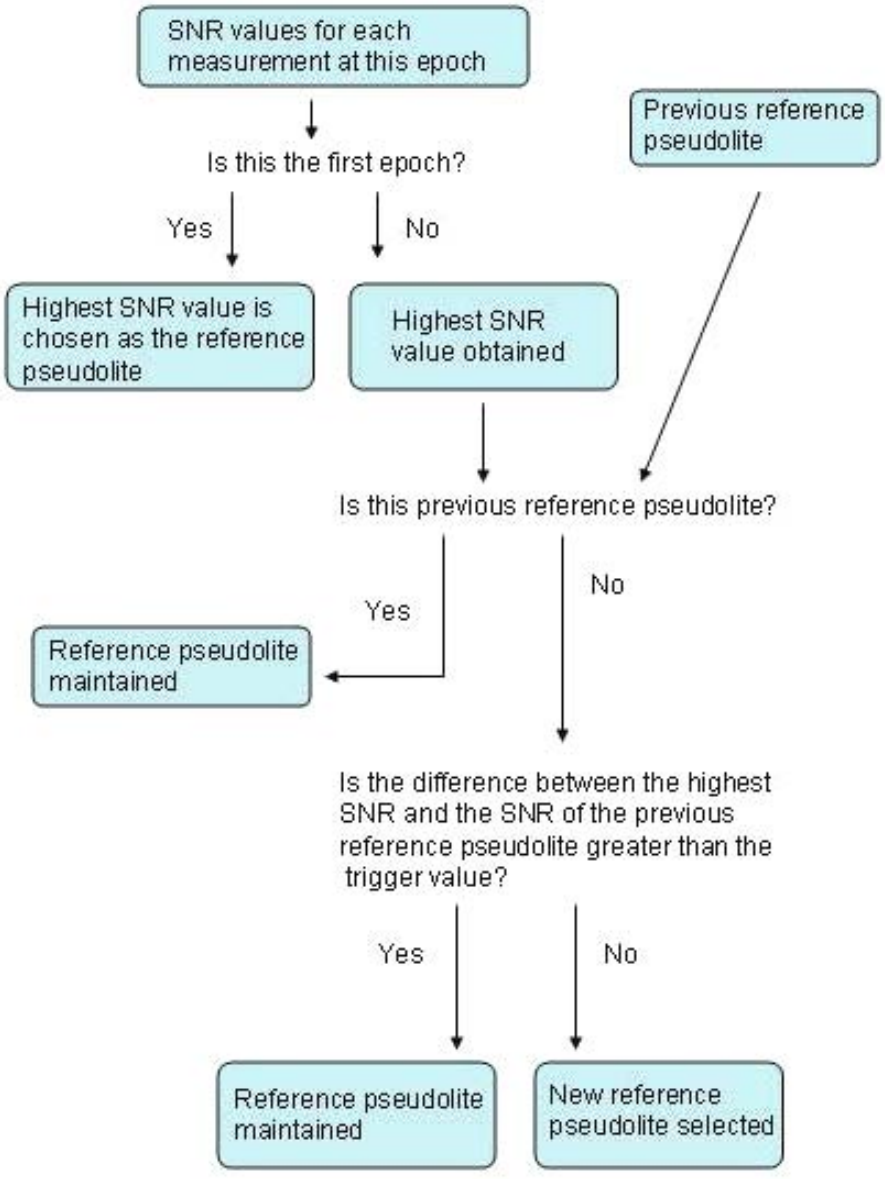

Figure 1. Reference Pseudolite Selection Algorithm Block Diagram

If pseudolite 1 was the reference pseudolite, then the solved values are:

$$N_{AB}^{12} = N_{AB}^{2} - N_{AB}^{1} \tag{5}$$

$$N_{AB}^{13} = N_{AB}^{3} - N_{AB}^{1} \tag{6}$$

$$N_{AB}^{14} = N_{AB}^{4} - N_{AB}^{1} \tag{7}$$

Let us now say that pseudolite 2 must become the reference pseudolite. The integer ambiguity values of the new reference pseudolite in terms of already solved terms can be found by:

$$N_{AB}^{21} = N_{AB}^{1} - N_{AB}^{2} = -(N_{AB}^{2} - N_{AB}^{1}) = -N_{AB}^{12} \tag{8}$$

$$N_{AB}^{23} = N_{AB}^{3} - N_{AB}^{2} = (N_{AB}^{3} - N_{AB}^{1}) - (N_{AB}^{2} - N_{AB}^{1}) = N_{AB}^{13} - N_{AB}^{12} \tag{9}$$

$$N_{AB}^{24} = N_{AB}^{4} - N_{AB}^{2} = (N_{AB}^{4} - N_{AB}^{1}) - (N_{AB}^{2} - N_{AB}^{1}) = N_{AB}^{14} - N_{AB}^{12} \tag{10}$$

Additionally, the covariance matrix was reset to the unnecessarily high initial values that made the filter sensitive to noise in the measurements. As a result, a change in the reference pseudolite was accompanied by a glitch in the good position fix of the rover. If we are to assume the measurements are independent, which appears to yield acceptable results while not necessarily rigorously correct, then new covariance values can be obtained by taking the root sum square of the two previous covariance values. Off-diagonal terms are set to zero under the assumption of independent measurements. The new diagonal covariance values are given as:

$$\sigma^{21} = \sigma^{12} \tag{11}$$

$$\sigma^{23} = \sqrt{(\sigma^{12})^2 + (\sigma^{13})^2} \tag{12}$$

$$\sigma^{24} = \sqrt{(\sigma^{12})^2 + (\sigma^{14})^2} \tag{13}$$

Additionally, another modification needed to be made to the simulation version of the code before testing and verification of the modifications could commence. Under the previous simulation methods, code and carrier phase measurements were returned, but there was no model in place to simulate the SNR values. The model implemented creates the observed behavior of SNR as a function of the receiver and transmitter locations. The model is a cosine function of the declination angle between pseudolite and receiver with a small random noise added to it.[11] The effect of which is to say that signal to noise ratios are high with pseudolites directly overhead, and decrease to the horizon as is typical of observed behavior. The equation for SNR is given in (14).

$$SNR = MAX\_SNR * Cos(\phi) + random \tag{14}$$

where ϕ is the declination angle, *MAX_SNR* is nominally chosen to be 20, and the random noise is Gaussian with a 1-σ value of 0.5.

Also, a more robust cycle slip detection algorithm was implemented. Though significant literature exists in the area of cycle slip detection, much of it relies upon additional measurements from sources such as inertial navigation sensors or dual frequency receivers.[2,15] Neither of these implementations were available for this application.

In the previous version of the code, a change in the double differenced carrier phase measurement greater than 5 meters was flagged as a cycle slip and the integer ambiguity reset based on the current position solution. With this style of cycle slip detection, two errors readily occur, as depicted in Figures 2 and 3. In the first, we see that the change in the double differenced measurements per epoch is greater than 5 meters which would flag cycle slips, yet in fact, no cycle slips occur. Though this is a possibility in a real world environment, it cannot happen in the lab because the entire range of acceptable motion is less than 5 meters. The second error, however, is one that could be encountered in the lab. Cycle slips clearly occur, but occur at a level below the 5-meter threshold, so they would be missed and not flagged as cycle slips.

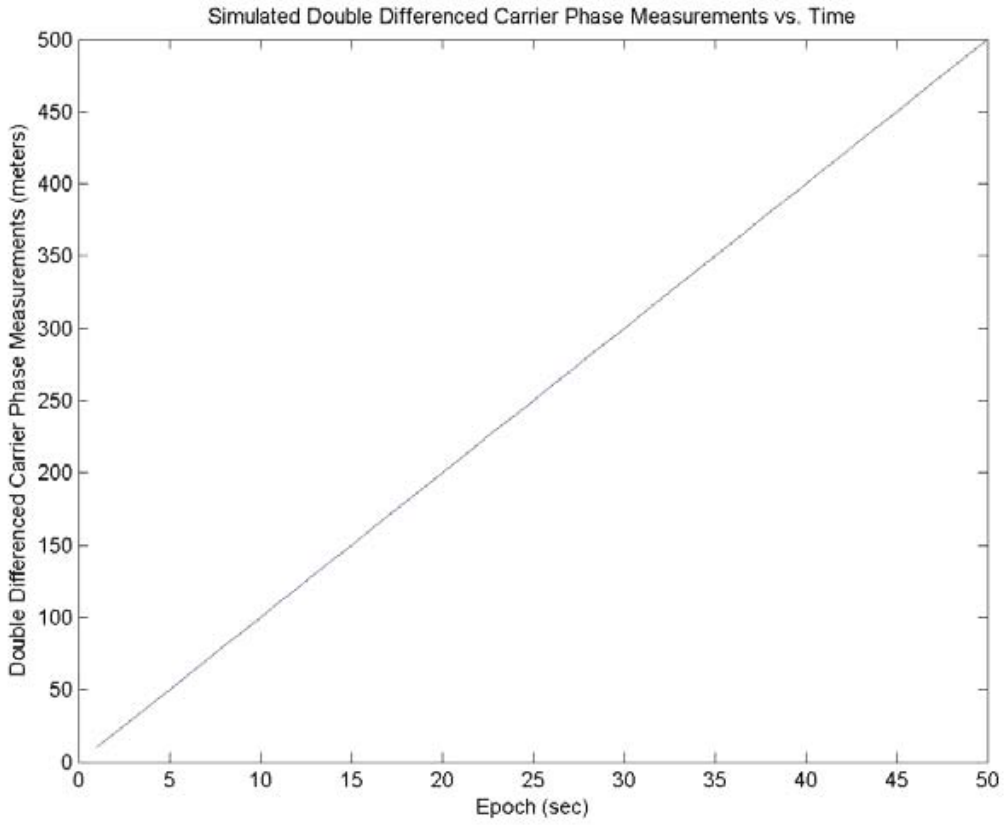

Figure 2. Example Of A False Cycle Slip Under The Old Detection Method

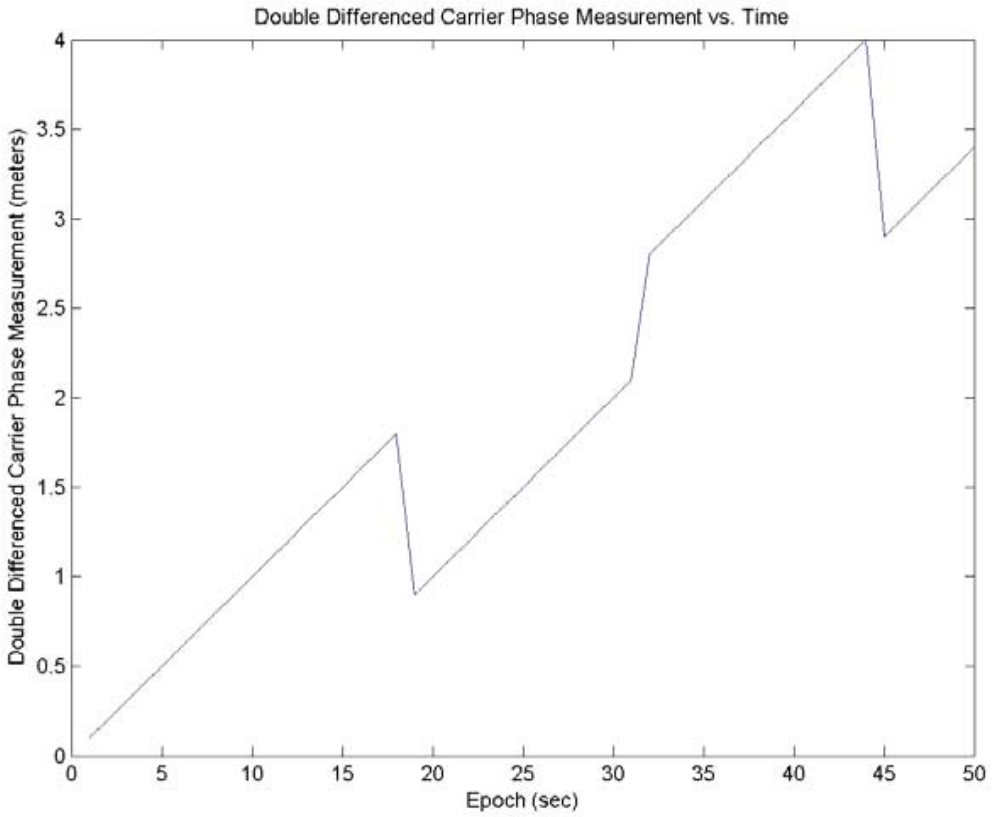

Figure 3. Example Of An Undetected Cycle Slip Under The Old Method

Under the new code, the previous epoch's change in the double differenced carrier phase measurements was used to project what the new measurement should be. Though still not entirely robust, the requirement that a smooth and continuous slope of the double differenced carrier phase measurements must be satisfied is an improvement over the previous detector. If the difference between the new epoch's measurement and the predicted measurement is too large, nominally 0.5 meters, a cycle slip is flagged. This criterion must be chosen with great care because a mark set too low will falsely flag some large motions where a cycle slip has not occurred. A mark set too high will not detect many smaller cycle slips. Some of the smallest possible cycle slips are extremely difficult to detect as they easily blend in with receiver motion.

To remove the cycle slip, the number of wavelengths of difference between the predicted and observed double difference measurement is added to the integer ambiguity for that double differenced pseudolite combination in the state. A block diagram of this new detector is included in Figure 4.

Lastly, in the time since the work of Wawrzyniak and Smart, a few of the pseudolites available for testing at the NSTL were known to be unusable at the time of testing. As a result of this hardware limitation, insufficient signals would be available to create a 3-dimensional solution. To accommodate this, the code was altered to only estimate a position

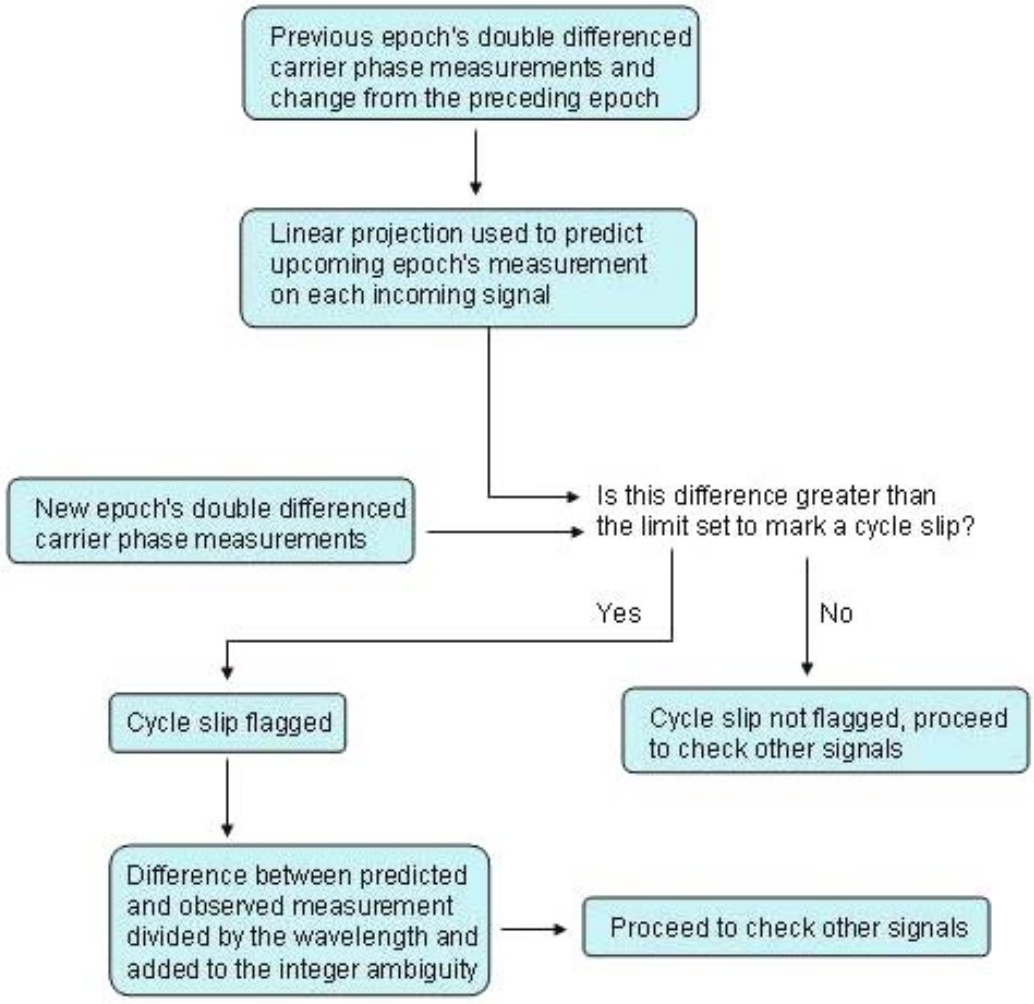

Figure 4. Cycle Slip Detection Algorithm Block Diagram

in 2-dimensions, the horizontal plane, while the vertical dimension was fixed to be constant at a known height. An overview of the entire processing code is presented in Figure 5.

2.4 TESTING OF THE MODIFIED CODE

With the modified code completed, testing of its capabilities began. As it was desired to test the modified code and simulate the type of results that could be achieved in the NSTL environment, the pseudolite locations and the trajectory that would be used in the lab were also used in simulation. In anticipation of testing at the NSTL, the pseudolites used in the simulation were A, C, D, and F. Their locations within the NSTL are displayed in Smart[10] and also below. Trajectories in the laboratory are now created with a robot arm. A top-down view of the important features in the laboratory is presented in Figure 6. Though a height dimension is not included on this plot, the reference and rover receivers are

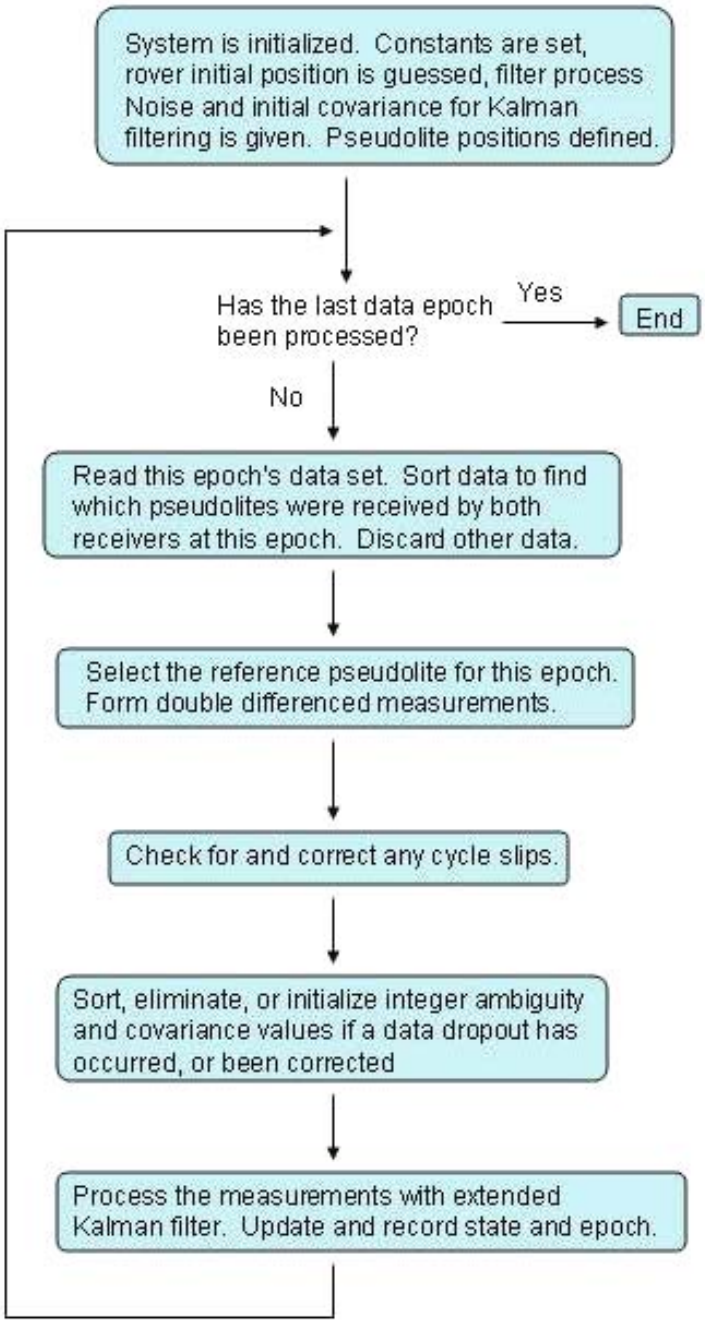

Figure 5. Block Diagram Of Processing Code

approximately 1 meter above the ground. Receivers C, D, and F are mounted to the side walls of the laboratory between 3 and 4 meters above the ground. Finally receiver A is hung from the ceiling of the lab about 8 meters above the floor. This gives a geometric dilution of precision (GDOP) at the origin of 1.55.

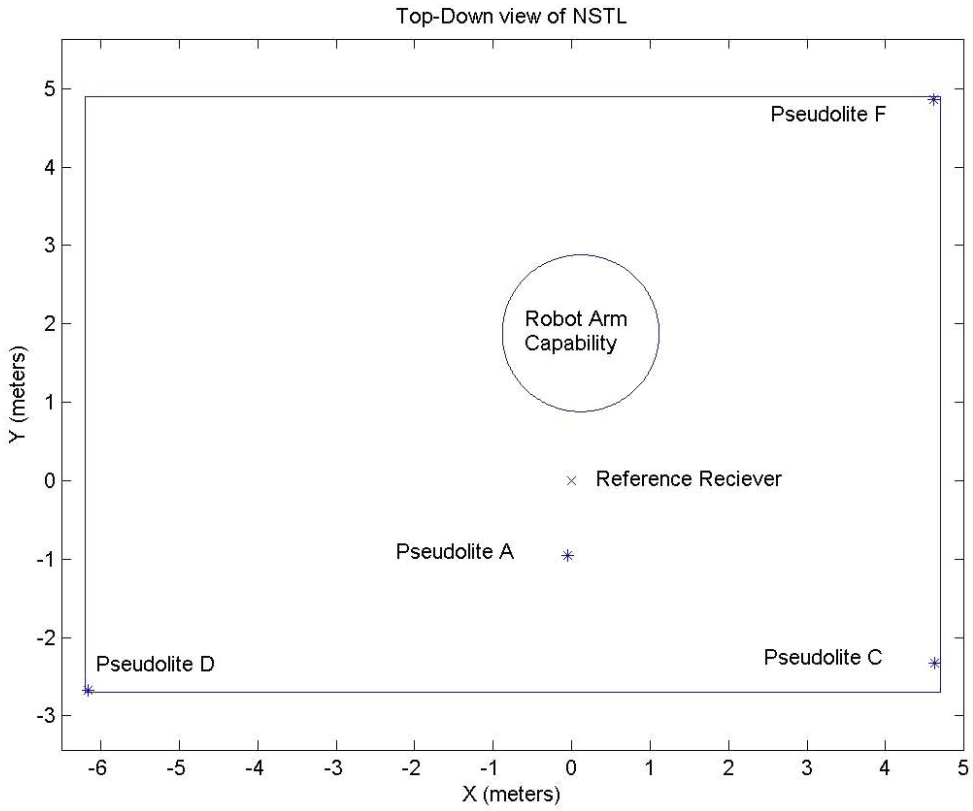

Figure 6. Overhead View Of The NSTL

The first simulation performed used simulated data generated without cycle slips or data dropouts. The trajectory followed by the rover receiver was 2 full rotations in a counterclockwise direction followed by a hard stop and a reversal in the opposite direction for the same angular displacement. This trajectory was selected as it represents the largest range that can be created by the robot arm with the limited length of electrical power supply cords that wrap around the center post of the robot arm. The angular velocity was selected to be 15 degrees/sec, a speed that nears the upper design limits of the robot arm. Based on previous work at the NSTL, the 1-σ value for the Gaussian noise on the carrier measurements is 4 mm. The results of that simulation are displayed in Figures 7-10.

In Figure 7, it is seen that the algorithm acquires a good fix on the receiver's position after about 1 minute, or 60 epochs, of data collection. This length of time is greatly varied with the process state noise values used to tune the extended Kalman filter, the initial error in predicted state, and the initial covariance values. In this example, the initial error of the receiver's position was on the order of 1 meter. The initial covariance and process state noise values used tended to yield acceptable results for a variety of simulations, but are not optimized. After the initial 60 seconds, the filter is able to maintain a lock on the rover's position to better than 10 cm of accuracy throughout the remainder of the 500 epoch simulation. Figures 7 and 8 illustrate this.

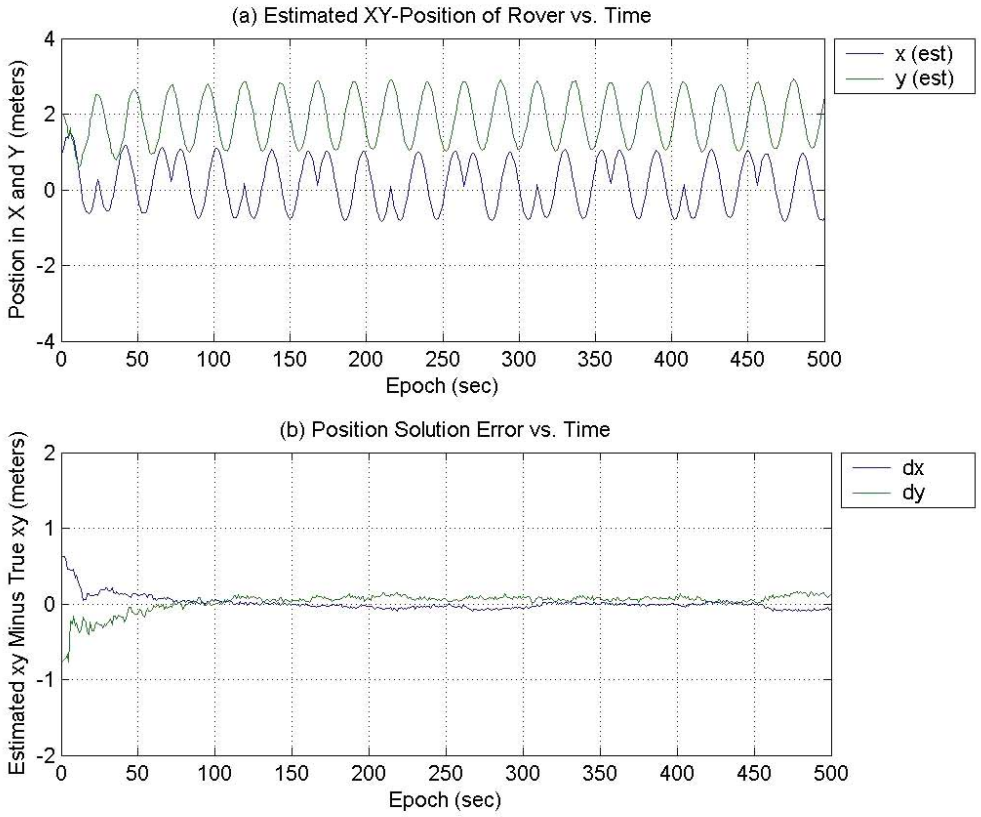

Figure 7. Accuracy Of Results From The First Simulation

Figure 9 shows the expected raw carrier phase measurements when no cycle clips are present. The trend of the measurements is due to the difference in the clock drift between the two receivers. Of course, due to the double differencing technique performed on the measurements, those trends are removed from the plot in Figure 10. In Figure 10, it should be noted that the value of the double differenced carrier phase measurement at the first epoch was subtracted from the double differences so that the structure of all three incoming data signals could be seen.

With this portion of the code validated, cycle slips were systematically introduced in the incoming measurements. In this test, cycle slips too small to have been detected by the previous algorithm are introduced at epochs 150, 250, and 350. The cycle slip at epoch 250 is on the reference pseudolite, while the other two cycle slips are on other pseudolites.

From this test, it is seen that cycle slips, whether they are on the reference pseudolite or one of the others, makes absolutely no impact on the accuracy of the position solution generated provided the slips are correctly detected and repaired. Figures 11 and 12 are identical to the previously displayed Figures 7 and 8, as we should expect if all cycle slips are correctly detected and removed. This is accomplished despite the notable difference in the double differenced carrier phase measurements portrayed in Figures 10 and 14.

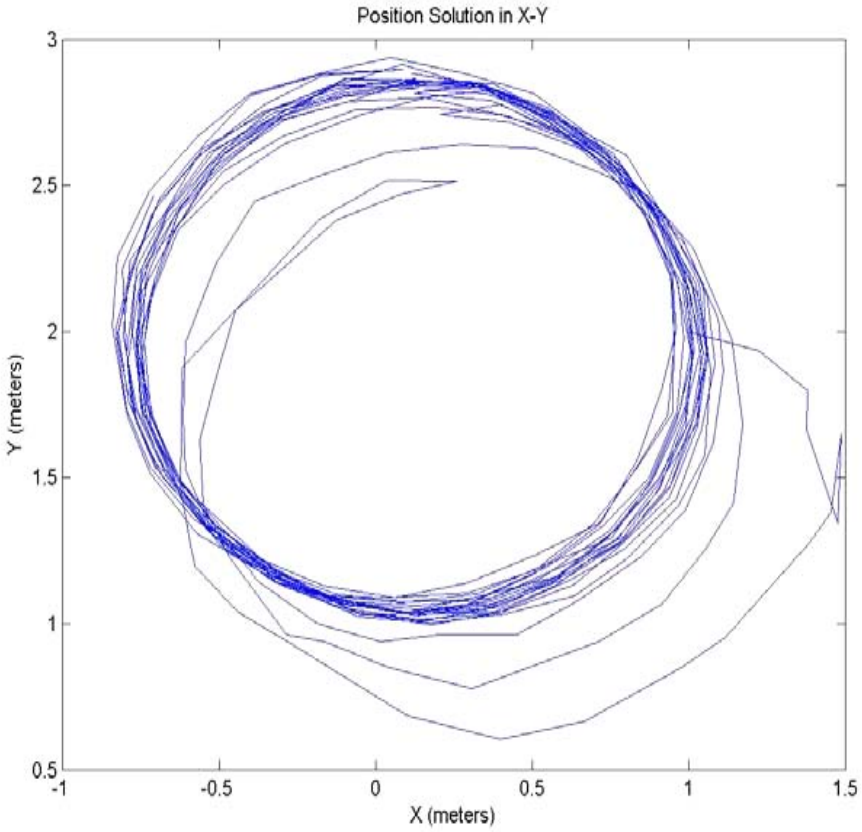

Figure 8. X-Y Plot Of Position Solution Generated

In this simulated model of the NSTL, a wide enough range of motion is not generated to cause a pseudolite C, D, or F to have a lower declination and hence stronger SNR than pseudolite A. Therefore, to test the reference pseudolite switching capability, a flag had to be inserted manually to select the reference pseudolite at a given epoch. With this means of forcing the reference pseudolite, the solution was yet again virtually unchanged, and the results appear strikingly similar to the first two simulations illustrated.

Based on the simulations demonstrated, as well as numerous others performed by Wawrzyniak and Smart not depicted here, a robust code has been developed which can dynamically accommodate the cycle slips, reference pseudolite switching, and data dropouts expected in the NSTL environment.

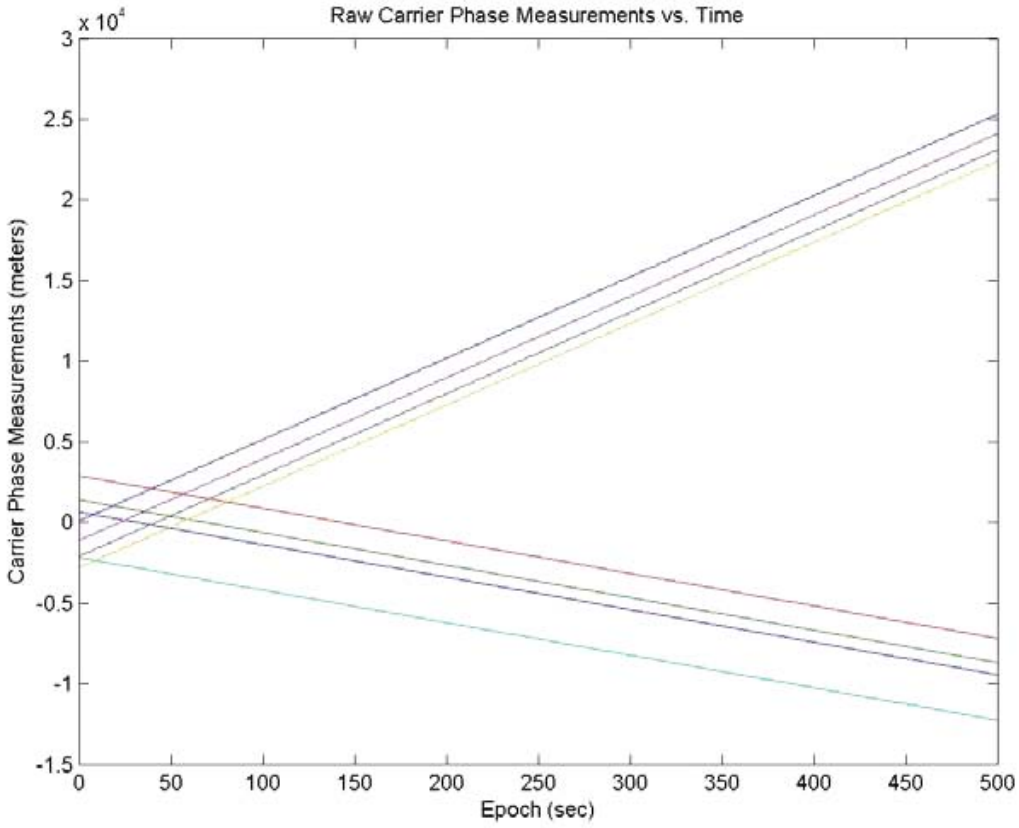

Figure 9. Raw Carrier Phase Measurements Over Time

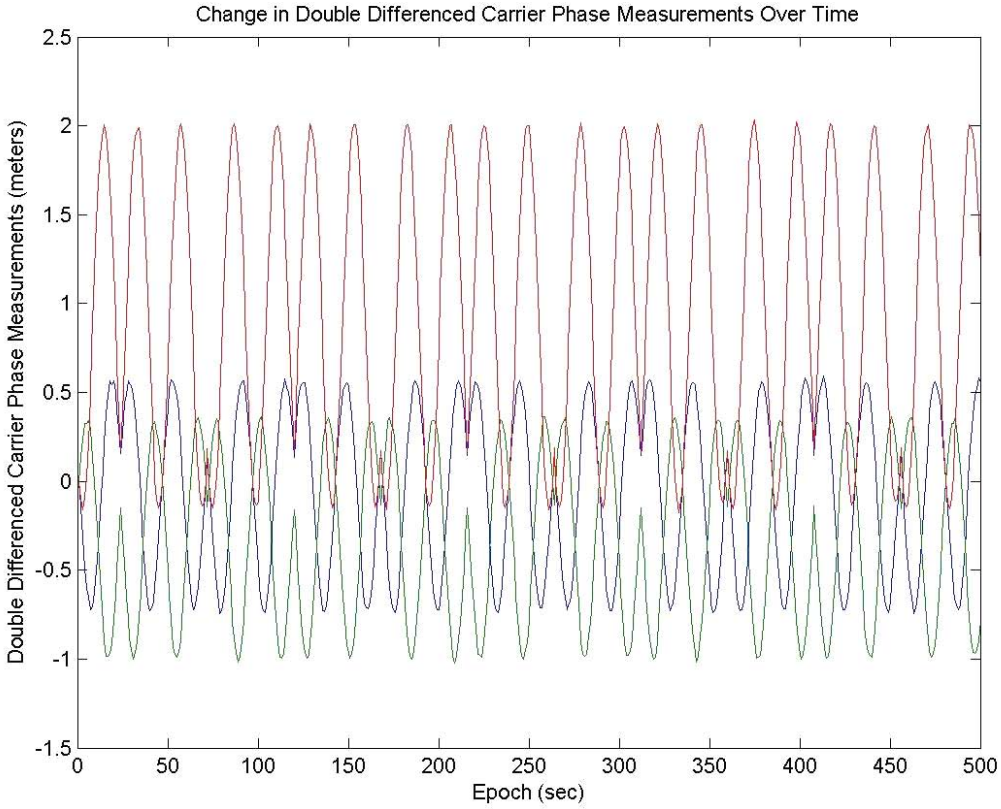

Figure 10. Double Differenced Carrier Phase Measurements

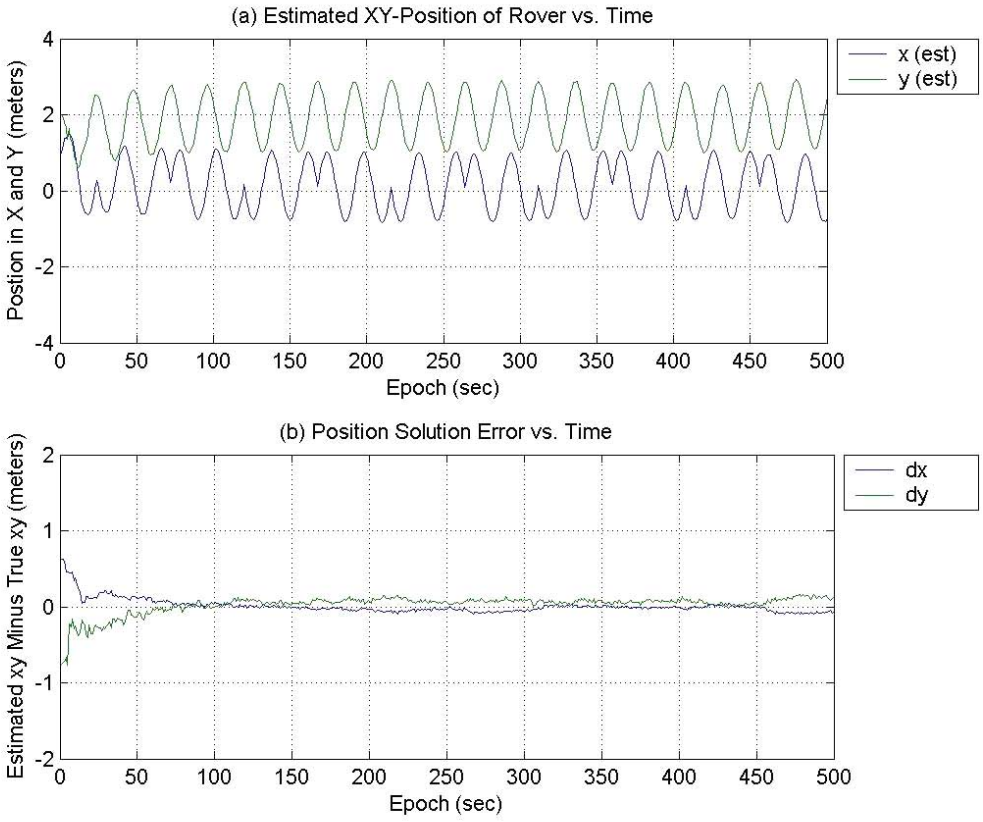

Figure 11. Position Solution Results From The Second Simulation With Cycle Slips Inserted

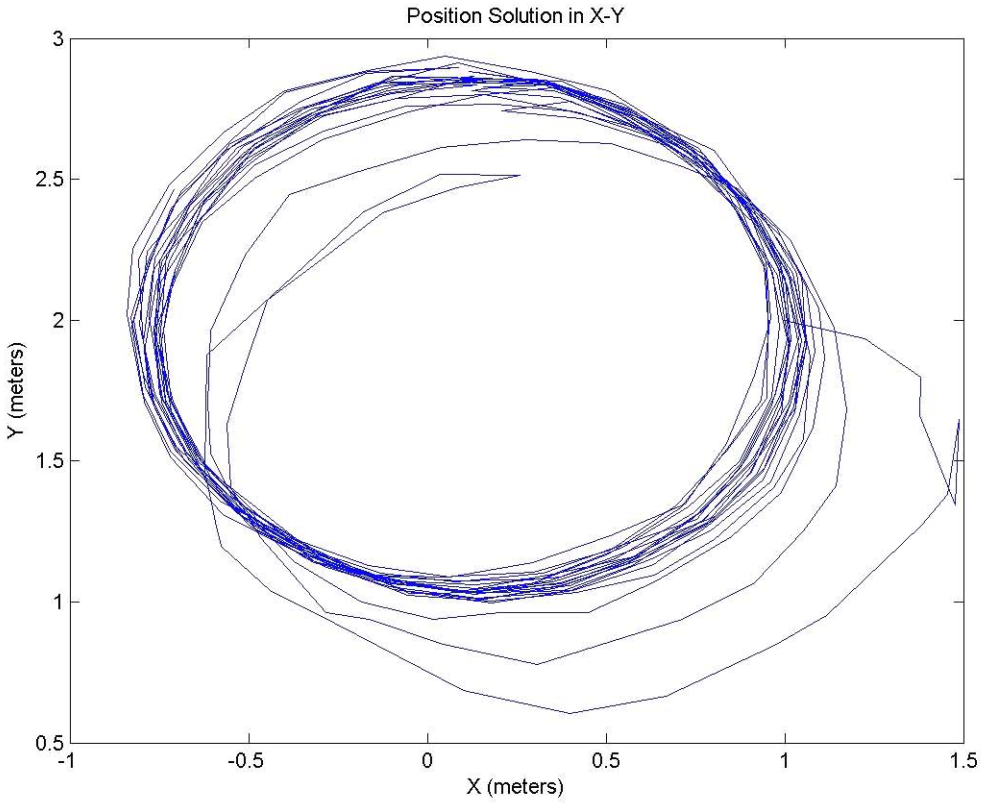

Figure 12. X-Y Plot Of Position Solution Generated With Cycle Slips Present

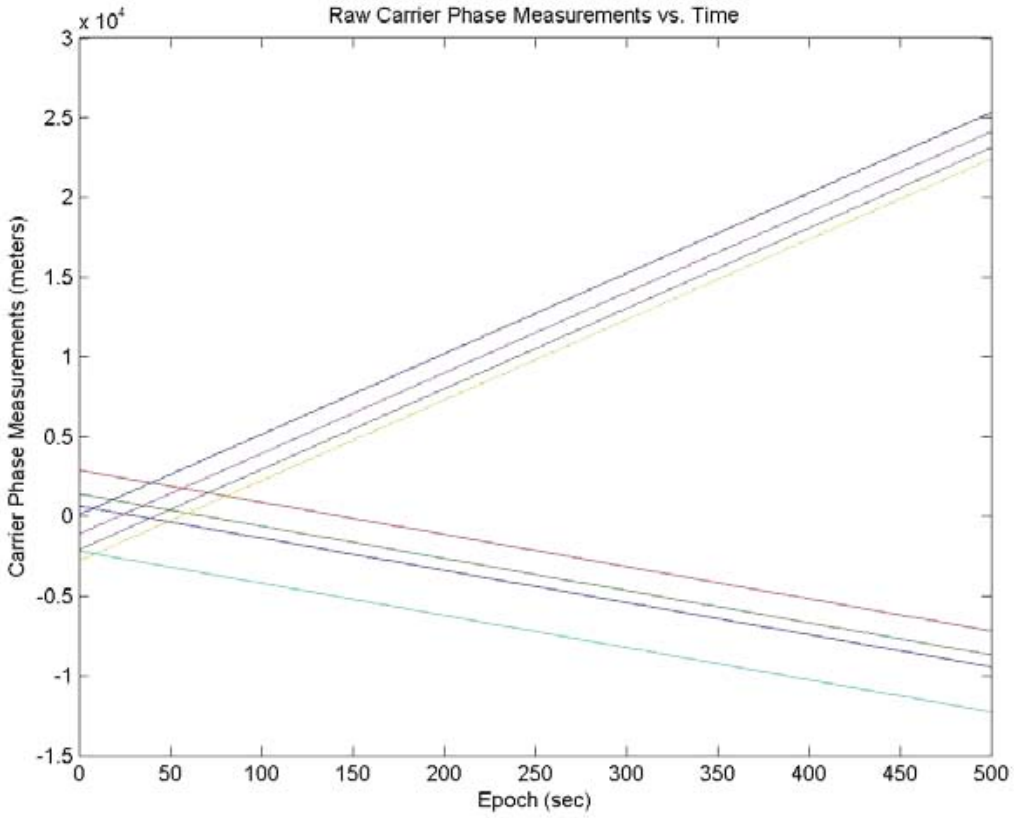

Figure 13. Raw Carrier Phase Measurements Over Time With Cycle Slips. Note: Cycle Slips Too Small To Be Seen On This Scale

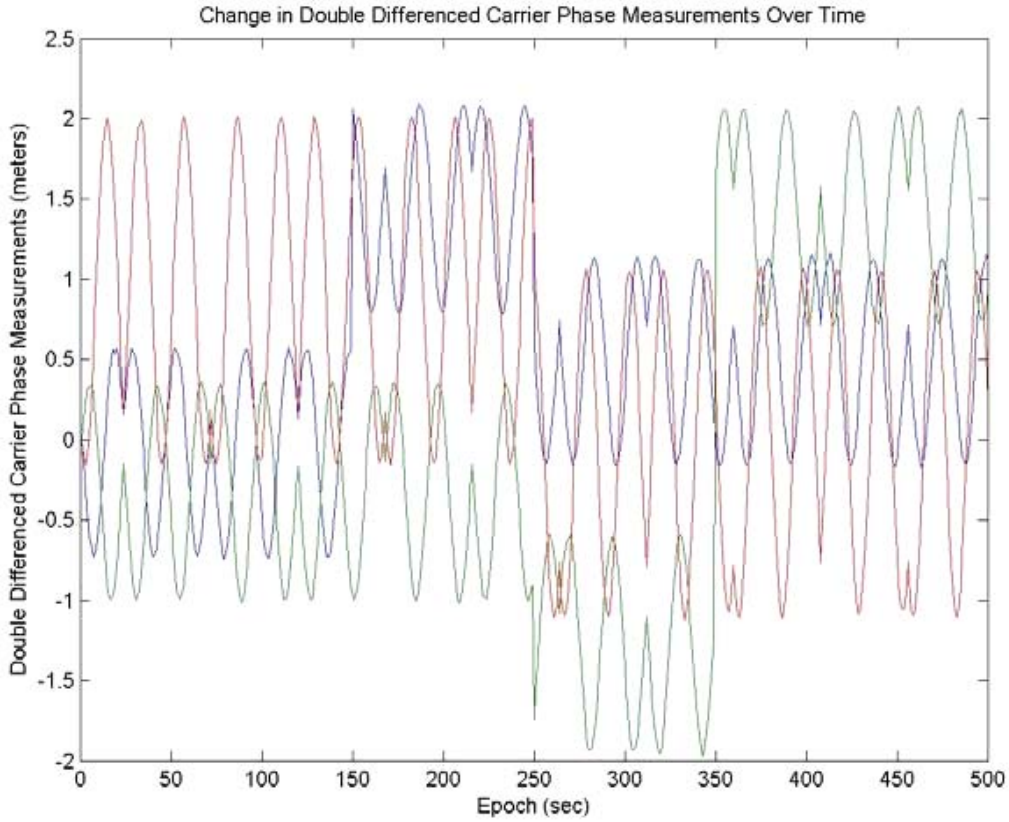

Figure 14. Double Differenced Carrier Phase Measurements With Cycle Slips

This page intentionally left blank.

CHAPTER 3
CODE VALIDATION ON EXPERIMENTAL DATA

3.1 PREVIOUS DATA COLLECTION

In May 2001, Smart collected data at NASA's Johnson Space Center to test the algorithm's ability to process real data in a post-processing fashion, in addition to its already proven ability to process simulated data as demonstrated by Wawrzyniak. Due to problems in the past with large amounts of noise on the measurements and difficulties with multipath in the NSTL, Smart collected data in an anechoic chamber at JSC.

At the time of Smart's data collection, 6 pseudolites were operating properly. Since this data was collected in the anechoic chamber instead of the NSTL, the robot arm was not available to generate the trajectory of the roving receiver. As a result, the motion of the rover had to be generated by hand. Based on conversations with Kevin Key of the LinCom Corporation who helped Smart perform her testing and data collection at NASA, Smart generated her motion by rotating in semi-circles and slowly raising the receiver from ground level to above her head.

3.2 PROCESSING PREVIOUS DATA

In a measure to validate the code with real data before attempting to process measurements in real-time at the NSTL, the new codes were run on the previously collected data. The difference between this version of the analysis and the previously completed post-processing is that data dropouts cannot be interpolated and selection of the reference pseudolite must be done on the fly as opposed to chosen by the user after looking at the entire data set. These capabilities make the current algorithm more suitable for a real-time implementation.

Since this data was generated by manual motion, there is no "truth" trajectory that has been recorded with which the solution of the rover's trajectory can be compared. As such, it is not known precisely how accurate the solution generated with this data and these algorithms is. What can be verified from this test is that the code runs properly on real data and in a real-time manner and that the trajectory computed by the algorithm makes sense from the knowledge of the trajectory followed by the receiver.

Since this trajectory was created when a sufficient number of pseudolites were available and the motion has components in three dimensions, a three-dimensional extended Kalman filter must be used for this aspect of the processing. This is the only difference

between the processing methods of this test and the simulations performed previously which were meant to imitate the conditions currently existing in the NSTL.

3.3 RESULTS OF REAL DATA PROCESSING

It is seen in Figures 15 through 18 that not only does the algorithm process the experimental data in a real-time manner as hoped, but that the trajectory computed by the algorithm does match what was anticipated. The receiver is completing half-circles of rotation with a radius of about 1 meter while steadily rising to a height of about 2 meters in the vertical direction. In looking closely at the plot of the double differenced carrier phase measurements, it can be observed that the noise on this data is even smaller than the 4 mm as was previously mentioned as being the expected value. In this case, the noise on the double differenced measurements appears to be closer to 1mm 1-σ in magnitude.

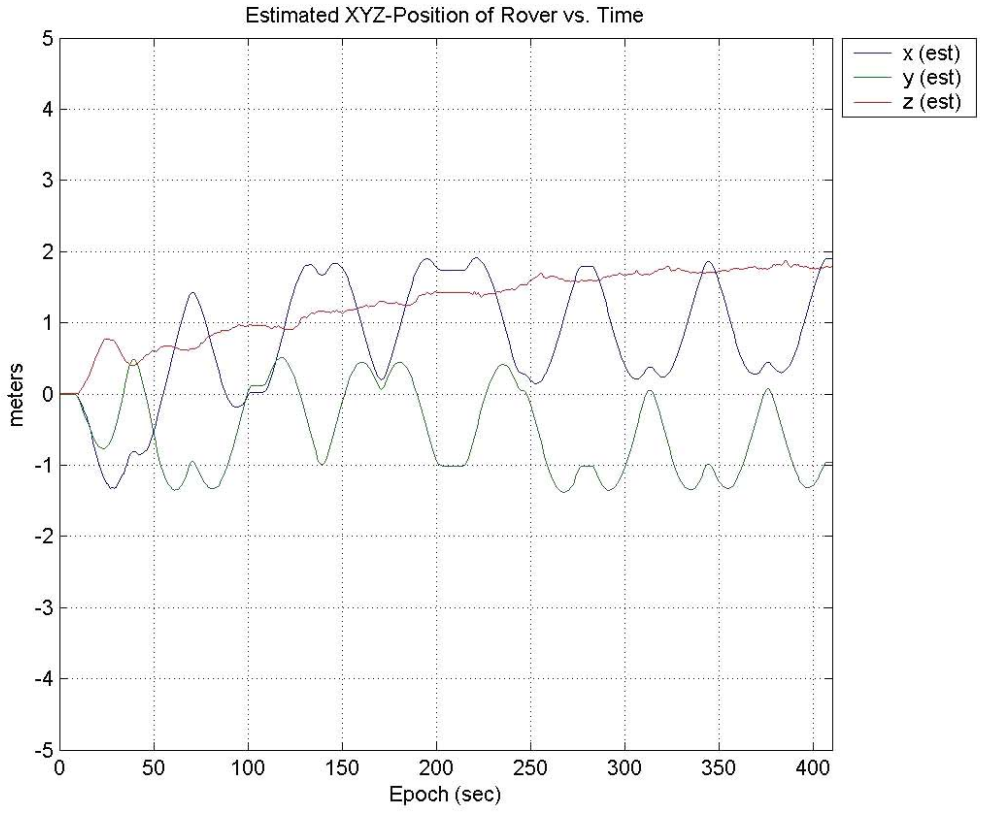

Figure 15. X, Y, And Z Positions Of The Rover Over Time

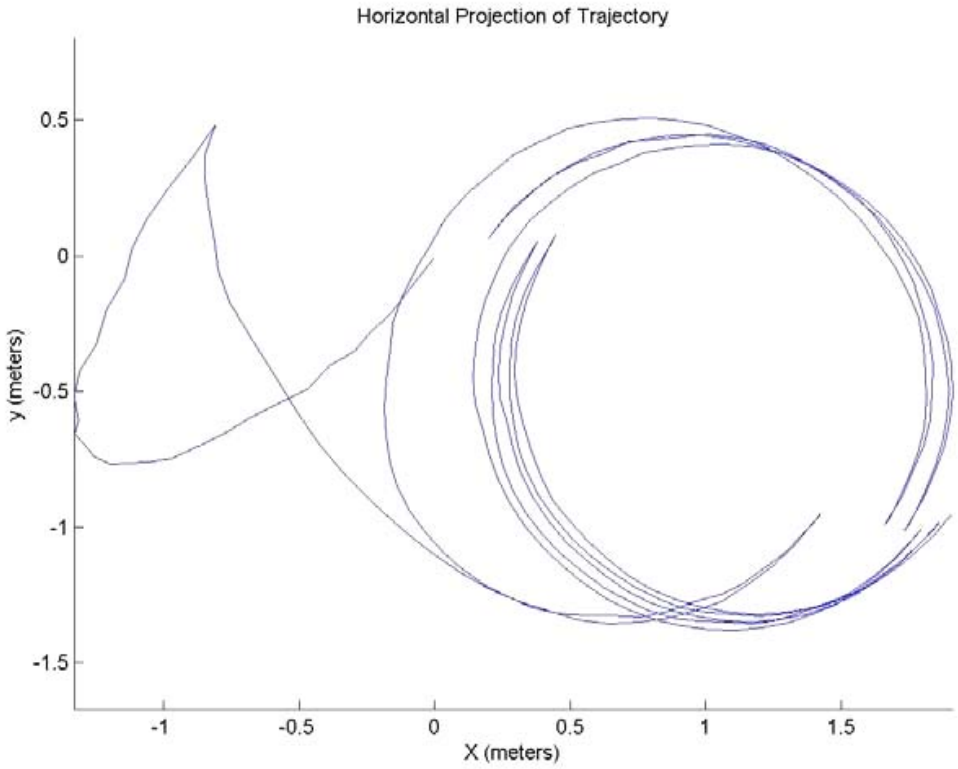

Figure 16. Horizontal Projection Of The Rover's Trajectory

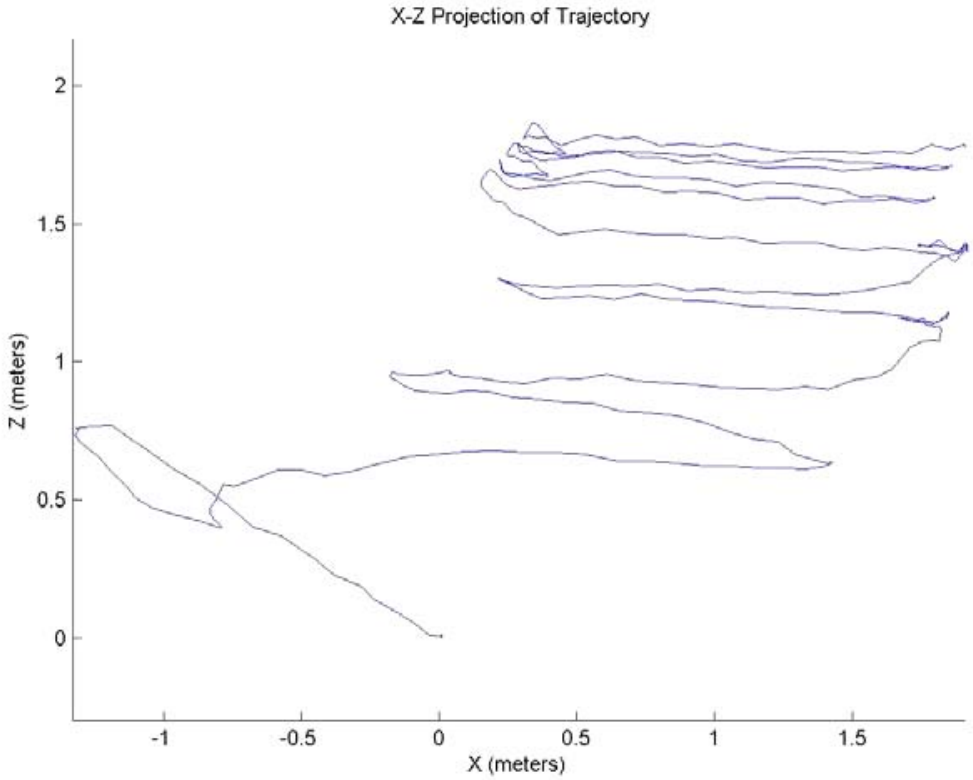

Figure 17. X-Z Projection Of The Rover's Trajectory

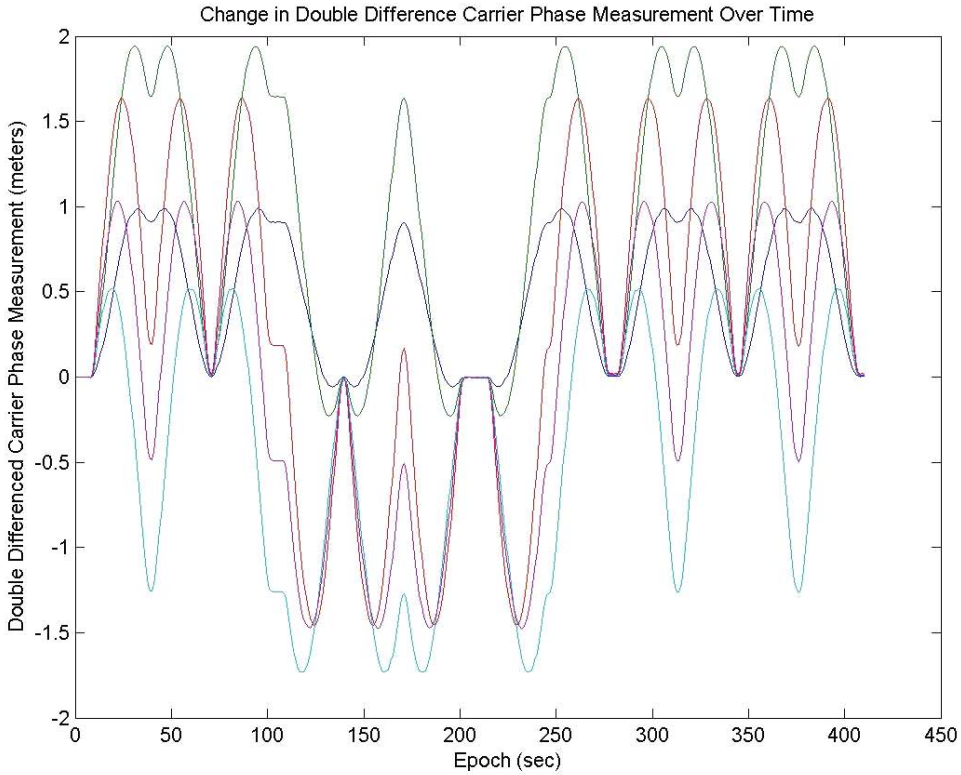

Figure 18. Change In Double Differenced Carrier Phase Measurements

This page intentionally left blank.

CHAPTER 4
REAL-TIME NAVIGATION IN THE NSTL

4.1 MOTIVATION FOR RETURNING TO THE NSTL

Although in Chapter 3 it was demonstrated that a real time capability has been accomplished, a demonstration of the algorithm along a known trajectory has not been achieved. Without that information, it is not known quantitatively how accurate the solution is. This goal was the motivation for returning to JSC to collect data in the NSTL where a truth trajectory could be generated and recorded by a computer controlled robot arm. With this known trajectory, a record of exactly how close the algorithm can come to accurately tracking a receiver in real-time can be found.

4.2 NSTL DATA COLLECTION

With significant assistance from Kevin Key of LinCom and Steve Provence of Boeing, both of whom work at JSC in the NSTL, the 4 remaining operational pseudolites were tuned to the greatest degree achievable. This was a matter of setting proper aiming direction of the transmitting pseudolites, setting the right inline attenuation, and setting proper pulse widths and durations. All these factors are critically important in achieving usable results. If a signal is too strong then the receiver has a high probability of locking onto a side lobe of the signal, or bleeding over to the other channels and corrupting those measurements as well. If the signal is not strong enough, then the signal is easily lost and data dropouts occur. The aiming direction of the transmitting pseudolites is very important as well. Since the receivers are in the near-field range of the transmitters with distances all below 10 meters, there are significant nulls, or regions of low SNR values, in the antenna gain pattern that will cause the receiver to lose lock when it passes through one of them. Only a finely tuned combination of these parameters on each of the transmitters will yield usable data. An example of one potential field of varying SNR values for a single pseudolite that could be encountered by the roving receiver is displayed in Figure 19.

Over the course of 2 days spent in the lab, 15 data files representing individual experiments were collected. In an attempt to maximize the chances of acquiring a data file with sufficient valid data for a good position solution, several parameters were varied through the tests. Tests were conducted with a variety of speeds and ranges of motions including no motion at all. Additionally, 2 different kinds of tracking loops were used in the receiver software in an attempt to collect data that did not contain an excessive number of cycle slips. A phase lock loop (PLL) that had been successfully used by Smart to obtain the

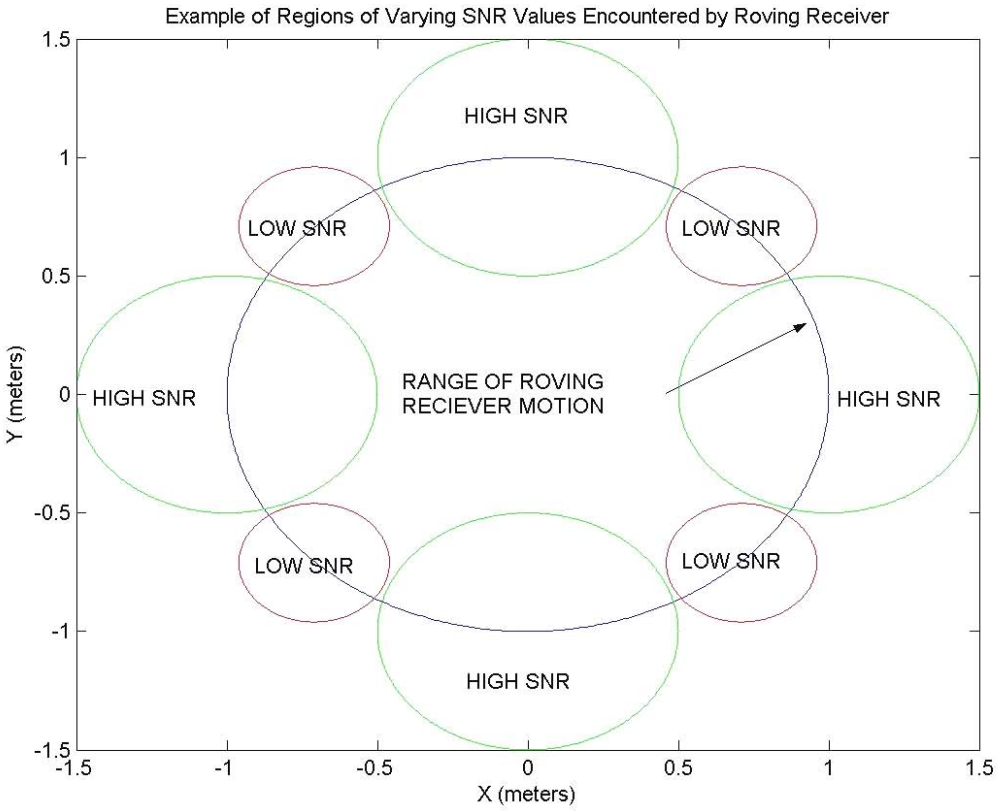

Figure 19. Example Of Regions Of High And Low SNR Values Encountered By The Roving Receiver As It Traverses Its Trajectory. Note That The Locations Of Low SNR Value Regions Are Different For Each Transmitting Pseudolite.

data in Chapter 3 and a frequency assisted phase lock loop (FLL/PLL) developed by Oliver Montenbruck that has been shown to yield better results in the past were used.

4.3 NSTL DATA PROCESSING

As an initial test of the calibration of the equipment, a data collection was conducted with no motion of the receivers. Though this test cannot be used to obtain a position fix of the receiver because the carrier phase extended Kalman filter requires motion to resolve position and integer ambiguity values, this test can show the type of data expected in other tests where motion of the rover does exist.

Figure 20 shows the double differenced carrier phase measurements without a cycle slip detector incorporated in the algorithm after the signals have been shifted so that the initial value is zero to accommodate displaying all signals on the same plot. When the cycle slip detector is not activated, a large number of clearly distinguishable cycle slips are observed. In this case, it turns out that while one signal has a large number of slips, the other two signals are relatively clean, displaying only a single cycle slip. From experience with

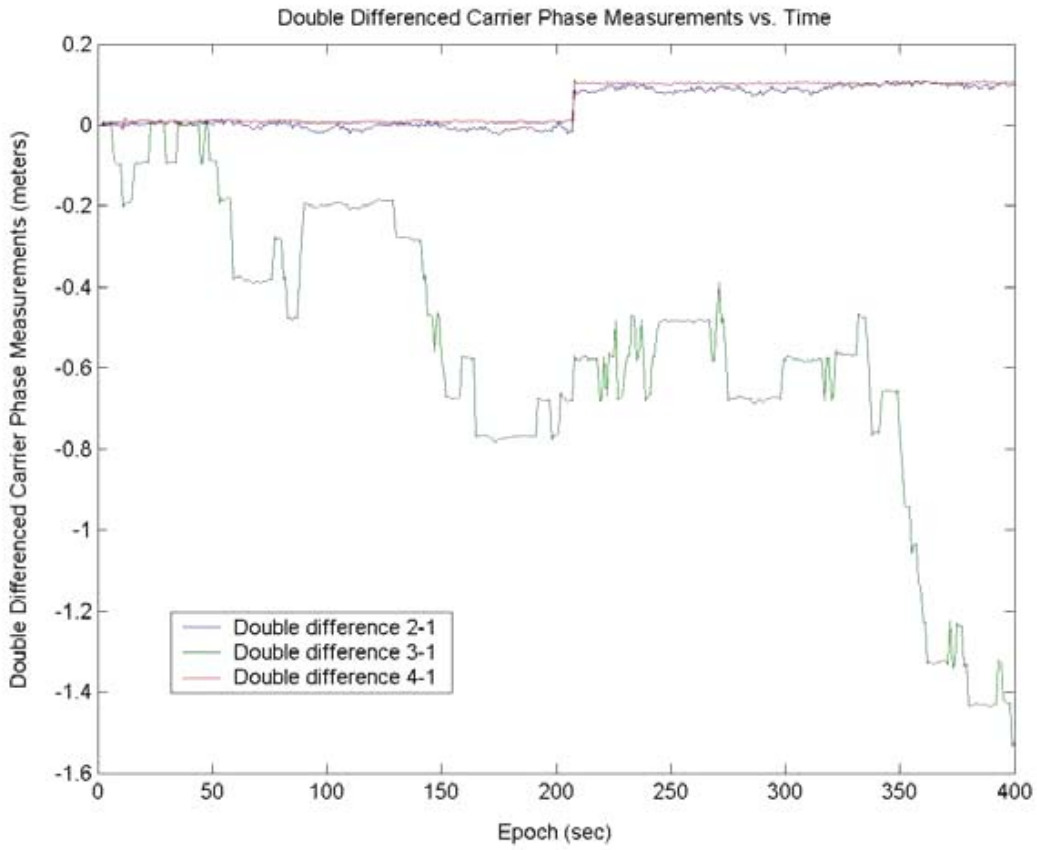

Figure 20. Double Differenced Carrier Phase Measurements Without Cycle Slip Detection

previous behavior in the laboratory, it is unusual that two of the signals have as few cycle slips as they do for that duration of time.

In this case it is also fortunate that the cycle slips are clear and discrete. This facilitates a relatively straightforward detection and removal of the slips. Using a cycle slip detector that shifts the remainder of the signal an integer number of half wavelengths, the smallest cycle slip allowed in the data with the current version of receiver software, Figure 21 was generated with cycle slips removed. Unfortunately however, in order to detect the majority of the cycle slips and generate this clean plot, a 5 cm criterion was required. This criterion had to be used because of the large number of cycle slips with small magnitudes. Though this means of cycle slip detection does resolve and eliminate all cycle slips in this example, the very fine 5 cm resolution required to accomplish that creates problems with the other experiments to follow.

Figures 20 and 21 begin to give an insight into a critical issue with real-time navigation in the NSTL environment with the hardware and software used. While the simulations performed in Chapter 2 incorporated simulated cycle slips, all the cycle slips were of a sufficiently large size in comparison with the velocity of the receiver. In the preceding example, no difference should be observed in the double differenced

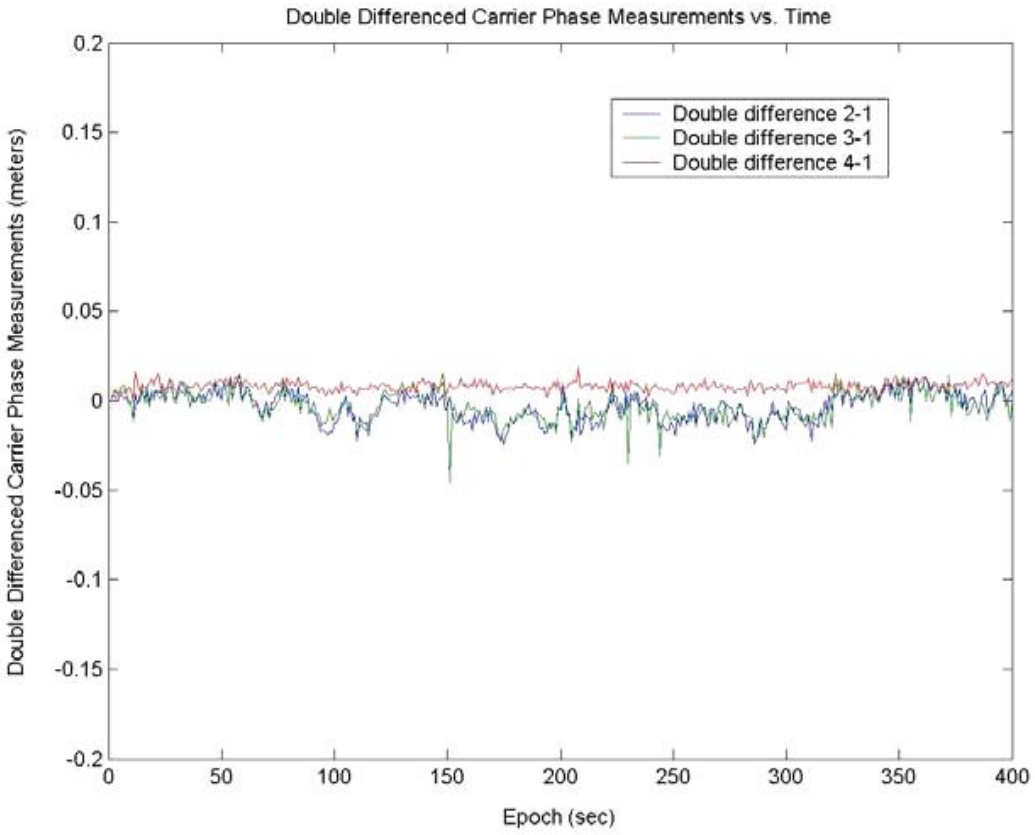

Figure 21. Double Differenced Carrier Phase After Cycle Slip Removal

measurements from one epoch to the next because there was no motion in the receivers. This result greatly facilitates the detection and removal of cycle slips by allowing a very small criterion to be used.

When the algorithm is employed to attempt to track the roving receiver while it is moving along a trajectory however, problems arise. If the rover has a very small velocity, which would help in the cycle slip detection routine, then passage through a null as mentioned earlier will almost certainly cause the receiver to lose lock on a signal, because it takes a long time for the receiver to pass through that area. After lock is lost it takes quite a long time for it to reacquire the signal. With only 4 pseudolites available, sufficient data no longer exists to observe and track the roving receiver after passing through nulls of just 2 pseudolites

As such, any usable data file, from a point of view of maintaining lock on the pseudolites, must have a velocity greater than that which would indicate a cycle slip has taken place. This being the case, cycle slips appear to be random noise on the double differenced measurements instead of the large discrete jumps that stood out so clearly earlier.

An example that clearly illustrates the difficulties of trying to detect cycle slips when they are of the same size as the velocities has been encountered and identified on a few

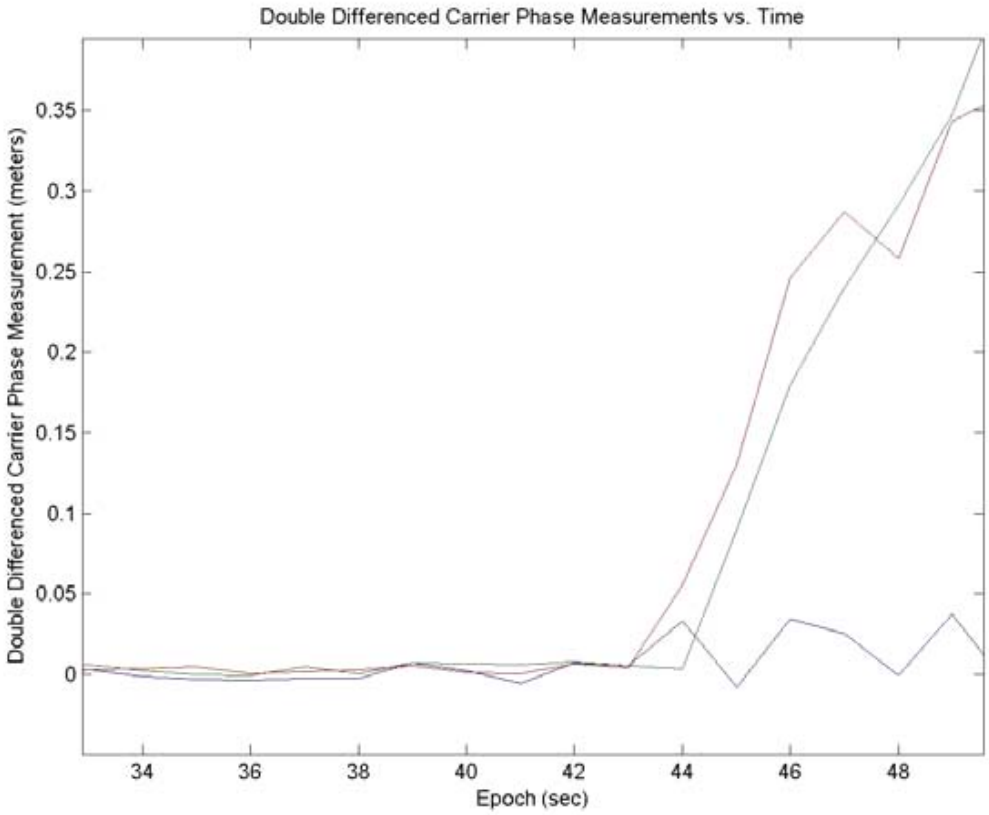

Figure 22. Double Differenced Carrier Phase Measurements. Note The "Hidden" Cycle Slips On The Blue Signal At Epochs 45, 47, And 48

occasions and has likely occurred several other times as well without being previously documented. As the roving receiver moves, a predictable change in the double differenced carrier phase measurements should accompany that. On occasion however, a cycle slip will occur of roughly equal magnitude but opposite direction to the anticipated change in double differenced measurement. The net result is that a relatively flat line will appear as the double difference when in fact it is full of cycle slips. Though these could be detected if the trajectory was known ahead of time and used to predict what the measurements should be, this requires *a priori* knowledge of the trajectory and defeats the purpose of real-time navigation.

An example of one of these is presented in Figure 22. Based on knowledge of the trajectory followed, it is known that once the motion begins at epoch 43, all three double differences should have increasing values of a similar magnitude per epoch. This behavior is displayed by the red and green double difference signals, but the blue one appears to experience 3 half-wavelength cycle slips. Figure 23 shows the result if it is known that cycle slips occur at epochs 45, 47, and 48. This almost exactly matches the predicted double difference measurements given that the trajectory is known.

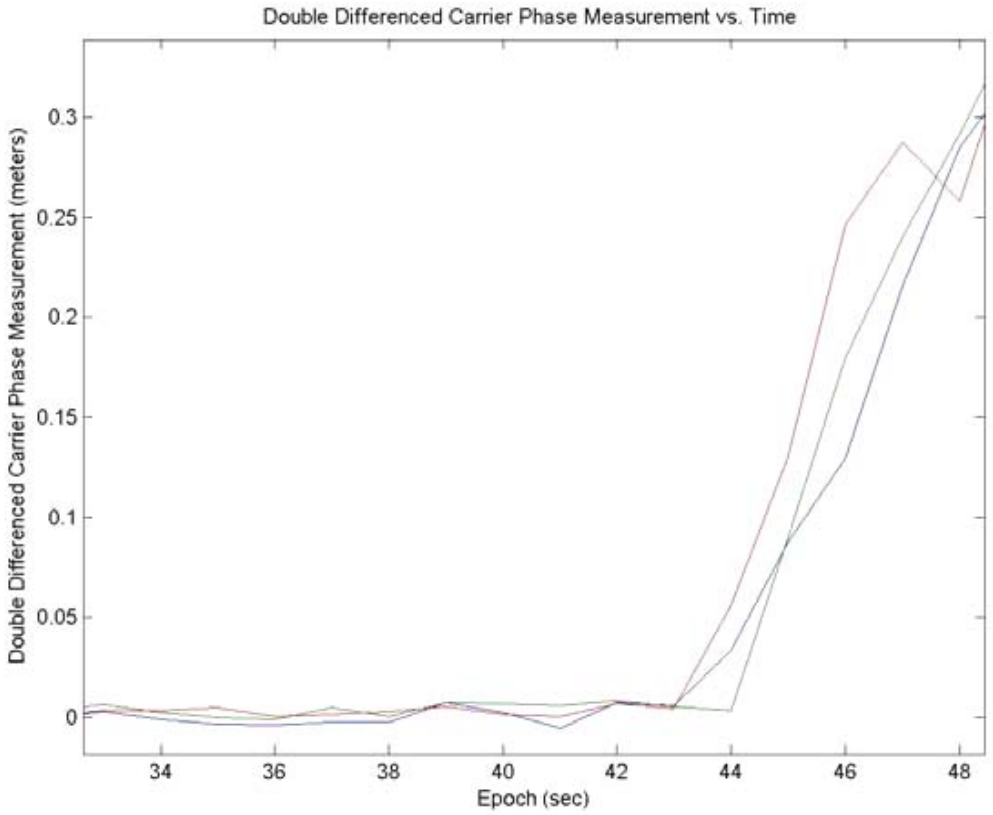

Figure 23. Double Differenced Carrier Phase Measurements "Hidden" Slips On The Blue Signal At Epochs 45, 47, And 48 Manually Removed

If it were possible to acquire a good fix on the rover's position and velocity then it may be possible to use a linear extrapolation method to predict the next measurement and flag it as a cycle slip if that measurement is greater than some criteria away than the predicted value. This is the method developed and described in Chapter 2. Unfortunately with the data collected, cycle slips are so frequent that it is not possible to acquire a good lock to being with. Since a good lock on the receiver's position cannot be acquired, this also prevents a reduction of the covariance values that could be used to detect cycle slips if the residuals grew substantially between epochs.

Another problem that has been observed several times is that a cycle slip will be clearly distinguishable in a signal, but it will take 2 epochs to develop. At this time, it is not known how that is happening but it does seem to indicate that some component of the tracking loops is not functioning as expected.

Figure 24 is an example of the numerous cycle slips that appear as noise with a bias that shifts over time, and makes cycle slip detection difficult. It also illustrates the large difference between the data collected by Smart in the anechoic chamber and the data collected for this work in the NSTL. This data was collected with the same PLL tracking loops and hardware as was previously employed. This particular plot was chosen because it

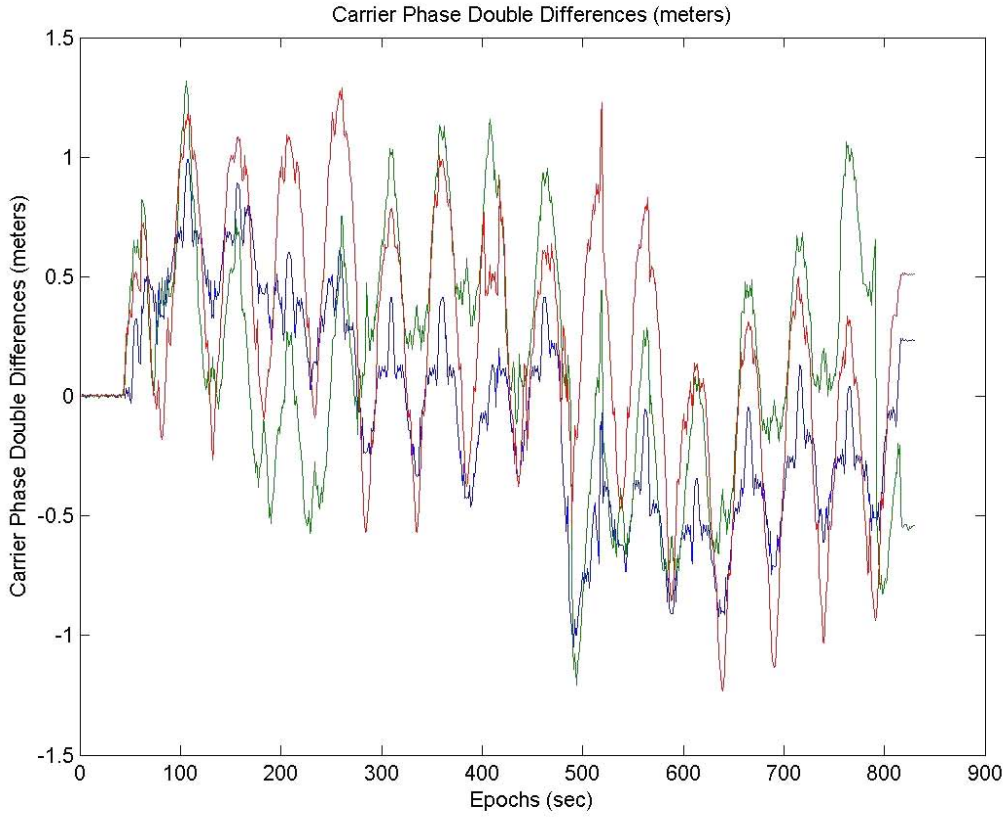

Figure 24. Double Differenced Carrier Phase Measurements. Note The Difference Between This Plot Of Data Collected In The NSTL And Figure 18, Which Shows Data Previously Collected In The Anechoic Chamber. Software Tracking Loops And Hardware Used Were Identical.

was one of the best examples available in terms of keeping lock on the pseudolites and a small number of cycle slips. The net number of cycle slips in this experiment can be found by looking at the beginning and ending values of the measurements, as the experiment was started and ended from the same location, so the measurements should be the same.

Additionally, this motion had a period of 50 seconds. That is to say the measurements should exactly repeat every 50 seconds. Though a generally repeating structure does exist, a time correlated drift, due to the large number of cycle slips, on the order of 1 meter causes the measurements not to repeat.

Processing this data with the cycle slip detectors mentioned previously set to filter different sizes of slips can be made to filter out a few of the larger jumps that can be seen in the picture. However, removal of those jumps does not eliminate all the cycle slips and does not substantively improve a position solution. As proof of this, the previously illustrated "hidden" cycle slip is demonstrated as a zoom of this plot. A hidden cycle slip such as this is

equally detrimental to an accurate position solution but has in fact no characteristic jump associated with it that could be observed by the filter without prior knowledge of the trajectory.

CHAPTER 5
CONCLUSIONS AND FUTURE WORK

5.1 SUMMARY OF RESULTS

Through the course of this work, two of the three previously stated goals were accomplished. An algorithm was developed that successfully processed both simulated and experimental data. This algorithm has demonstrated an ability to track a roving receiver to accuracy better than 10 cm in simulations and likely better than 1 meter processing previously collected experimental data.

Unfortunately, due to some combination of problems with the hardware, software, or environment of the NSTL, a demonstration of real-time navigation with a measure of the accuracy of its performance was not achieved. This could be due to problems with the receivers, either in hardware or software, pseudolites, signal generator for the pseudolites or other sources yet to be considered.

While other researchers have also found real-time navigation in the NSTL to be unachievable, their conclusion has largely been to attribute the lack of success to multipath within the NSTL environment. Though this may be a contributing factor, it appears that cycle slips may be a more important factor in this limitation. A comparison between Figures 18 and 24, may logically lead one to say that the measurements are much noisier in the NSTL and multipath could be a cause of that problem. However, that information coupled with the behavior seen in Figure 20 may raise the possibility that numerous cycle slips and not noise generated by multipath phenomena are a leading cause of the troubles thus encountered.

These numerous cycle slips which have prevented a demonstration of the real-time accuracy could be a result of many sources. Receiver hardware, built with off the shelf components, may have trouble tracking the signals in the noisy and dynamic NSTL environment. Similar troubles with the environment may plague the software tracking loops in the receiver. The small range between the pseudolite antennas and the receiver antennas puts them in the near field range. That causes large changes in the SNR values between epochs and may contribute to cycle slips. Similarly, the numerous nulls present in the near-field range could cause cycle slips to occur. The enclosed environment of the NSTL, which does not easily permit radiation energy to be dissipated, may be a contributing factor. Additionally, it is unknown at this time how the signal pulsing, which was required to reduce the SNR values to reasonable levels, affects the carrier phase tracking of the receivers.

5.2 FUTURE WORK

As just mentioned, it is the belief of this author that the largest difficulty to be overcome in achieving real-time navigation in the NSTL is cycle slip elimination. Previous discussions have illustrated how this problem is not one that can be easily resolved by the processing algorithm. As such, more work must be done in identifying the source of these cycle slips if a real-time demonstration is to be realized. It appears likely that cycle slips occur with greater frequency while the receiver is in motion, though no definitive conclusions can be drawn about this because of the previously described interaction between cycle slips and receiver velocity. This observation may be one clue in helping to identify the source of the problem, but does not clearly point to a single direction to look for the source of the cycle slips.

Several experiments could be conducted to begin to isolate and eliminate the sources of the cycle slip problem. The equipment could be moved to a much larger outdoor location where data would be collected again. This would likely eliminate problems associated with the enclosed NSTL environment, near field range problems such as dynamic SNR and nulls, and multipath. If the number of cycle slips is drastically tempered in that experiment, the range could be reduced, outside again, to help single out the largest contributing factor. If a near equal number of cycle slips remain, investigations should start to examine the hardware and software employed in the receivers and transmitters.

5.3 CONCLUSIONS

Though real-time GPS pseudolite-based relative navigation was not successfully demonstrated in real-time in the NSTL, it does not appear to be out of reach. As discussed and demonstrated in Chapter 2, an algorithm, robust when faced of reference pseudolite switching, data dropouts, and large cycle slips, has proven to be reliable and successful at tracking a roving receiver in simulation and in previously collected data. If the source of the cycle slips can be identified and removed, it appears likely that a real-time demonstration in the NSTL can be performed.

Such a demonstration would be important, as it would demonstrate the viability of the method for applications of interest to NASA such as the ISS/Space Shuttle rendezvous and docking problem, but also for a variety of terrestrial applications where precision navigation is required, but access to sufficient GPS satellites is not permitted.

Bibliography

[1] ARINC Research Corporation, "Navstar GPS Space Segment Navigation / Navigation User Interfaces", Drawing No.: ICD-GPS-200, Rev. C., El Segundo, CA, September 1997.

[2] Bisnath, S., Langley, R., "Automated Cycle Slip Correction of Dual-Frequency Kinematic GPS Data", Proceedings of the 13th International Technical Meeting of the Satellite Division of the Institute of Navigation (ION-GPS 2000), Salt Lake City, UT, September 2000.

[3] Cobb, H. S., "GPS Pseudolites: Theory, Design, and Applications", Doctoral Dissertation, Stanford University, September 1997.

[4] Cooke, M.P., S.F. Gomez, H.J. Yim, "NASA Johnson Space Center (JSC) / Port of Houston Authority (PHA) Global Positioning System (GPS) Heading Board Specification", NASA Johnson Space Center, August 4, 1999.

[5] Corrazini, T., How, J., "Onboard GPS Signal Augmentation for Spacecraft Formation Flying", Proceedings of the Institute of Navigation GPS-98 Conference, Nashville TN, September 1998.

[6] Hofmann-Wellenhof, B., H. Lichtenegger, and J. Collins, *Global Positioning System: Theory and Practice*, 4th ed., Springer, New York, 1997.

[7] IntegriNautics Corporation, "IN200C-XL General Purpose Pseudolite: Users Manual, Version 2.2", Menlo Park, CA, September 1999.

[8] IntegriNautics Corporation, www.integrinautics.com, Menlo Park, CA, 2002.

[9] Lightsey, E.G. Graduate Course ASE 389P.7 Lecture Notes, Global Positioning System, The University of Texas-Austin, Fall Semester 2002.

[10] Lightsey, E.G. "Spacecraft Attitude Control Using GPS Carrier Phase", in *Global Positioning System: Theory and Applications Volume II*, eds. B.W. Parkinson, J.J. Spilker Jr., P. Axelrad, and P. Enge, AIAA, Washington, D.C., 1996, pp. 461-480.

[11] Masden, J., "Use of Kalman Filtering Techniques on a Signal to Noise Ratio Attitude Estimation Algorithm for the International Space Station", Masters thesis, The University of Texas at Austin, August 2000.

[12] Misra, P., Enge, P., *Global Positioning System Signals, Measurements, and Performance*, Ganga-Jamuna Press, Lincoln, Massachusetts, 2001.

[13] Poole, S.R., Graduate Course ASE 381P.6 Lecture Notes, Statistical Estimation Theory, The University of Texas-Austin, Spring Semester 2002.

[14] Smart, T., "Relative Navigation Using Experimental Pseudolite Results at NASA's Johnson Space Center", Masters thesis, The University of Texas at Austin, May 2002

[15] Scherzinger, B., "Precise Robust Positioning with Inertial/GPS RTK", Proceedings of the 13th International Technical Meeting of the Satellite Division of the Institute of Navigation (ION-GPS 2000), Salt Lake City, UT, September 2000.

[16] Schutz, B.E., et al., "Dynamic Orbit Determination Using GPS Measurements from TOPEX/POSEIDON", Geophysical Research Letters, vol. 21, No. 19, Sept. 15, 1994, pp.2179-2182

[17] Stone, J. M., et al., "GPS Pseudolite Transcievers and Their Applications", proceedings of the 1999 ION National Technical Meeting, San Diego, January 1999.

[18] Tapley, B.D., B.E. Schutz, and G.H. Born, *Fundamentals of Orbit Determination*, Center for Space Research, The University of Texas-Austin and the Colorado Center for Astrodynamics Research, Academic Press, 2002.

[19] Turner A., J. Rodden, and M. Tse (Space Systems/Loral, Palo Alto, CA), "GPS Spacecraft Navigation for Oribt Determination and Satellite Constellation Control", AIAA Paper 2000-1226, AIAA International Communications Satellite Systems Conference and Exhibit, Oakland, CA, April 10-14, 2000, Collection of Technical Papers, vol. 2 (A00-25001 06-32).

[20] Wawrzyniak, G., "Relative Positioning Using GPS Pseudolites in the Navigation Systems Testing Laboratory at NASA's Johnson Space Center", Masters thesis, The University of Texas at Austin, May 2001

[21] Wheelock, C.B., "AERCam II", NASA Johnson Space Center website *http://ranier.hq.nasa.gov/telerobotics_page/FY97Plan/Chap2h.html#AERcam* , 1997.

Distribution

1	MS 0323	D. L. Chavez, 01011 (LDRD Office)
1	MS 0825	W. L. Hermina, 09110
1	MS 0825	W. P. Wolfe, 09115
1	MS 0841	T. C. Bickel, 09100
1	MS 1162	W. H. Rutledge, 15414
1	MS 1174	A. C. Watts, 15400
1	MS 1174	E. E. Creel, 15426
2	MS 0899	Technical Library, 09616
1	MS 9018	Central Technical Files, 08945-1

1 Eric Monda
511 W Mineral Ave
Apt 115
Littleton, CO 80120